TURUN YLIOPISTO
UNIVERSITY OF TURKU

DEVELOPMENT OF NAPHTHALENE DIIMIDE–BASED FLOW BATTERIES

Mahsa Shahsavan

TURUN YLIOPISTON JULKAISUJA – ANNALES UNIVERSITATIS TURKUENSIS
SARJA – SER. F OSA – TOM. 70 | TECHNICA – INFORMATICA | TURKU 2025

TURUN YLIOPISTO
UNIVERSITY OF TURKU

DEVELOPMENT OF NAPHTHALENE DIIMIDE–BASED FLOW BATTERIES

Mahsa Shahsavan

TURUN YLIOPISTON JULKAISUJA – ANNALES UNIVERSITATIS TURKUENSIS
SARJA – SER. F OSA – TOM. 70 | TECHNICA – INFORMATICA | TURKU 2025

University of Turku

Faculty of Technology
Department of Mechanical and Materials Engineering
Materials Engineering
Doctoral programme in Technology (DPT)

Supervised by

Professor Pekka Peljo
University of Turku
Turku, Finland

Professor Johan Hjelm
Technical University of Denmark
Kongens Lyngby, Denmark

Reviewed by

Assistant Professor Marc-Antoni Goulet
Concordia University
Montreal, Canada

Dr Florence Geneste
Rennes Institute of Chemical Sciences
Rennes, France

Opponent

Professor Elisabet Ahlberg
University of Gothenburg
Gothenburg, Sweden

The originality of this publication has been checked in accordance with the University of Turku quality assurance system using the Turnitin OriginalityCheck service.

ISBN 978-952-02-0475-4 (PDF)
ISSN 2736-9390 (Painettu/Print)
ISSN 2736-9684 (Sähköinen/Online)

The best way out is always through.

"Robert Frost"

UNIVERSITY OF TURKU
Faculty of Technology
Department of Mechanical and Materials Engineering
Materials Engineering
MAHSA SHAHSAVAN: Development of Naphthalene Diimide–Based Flow Batteries
Doctoral Dissertation, 103 pp.
Doctoral Programme in Technology (DPT)
Month Year

ABSTRACT

The transition to use more renewable energies is essential to mitigate climate change and to reduce the dependency on fossil fuels. However, the intermittent nature of solar and wind energies requires more efficient and scalable energy storage systems to ensure a reliable energy supply at demand. Flow batteries and particularly aqueous organic flow batteries, have emerged as a promising solution for stationary storage applications due to their inherent fire safety and more importantly due to their ability to decouple energy and power. Unlike traditional vanadium-based flow batteries, aqueous organic flow batteries utilize redox-active organic molecules that are attractive for their potential for low cost and synthetic tunability. In this thesis, we took two approaches towards the development of aqueous organic flow batteries. First, we studied the electrochemical properties and flow battery performance of two novel functionalized naphthalene diimides focusing on their solubility, redox behaviour and stability in the battery. Second, to address the self-association behaviour of organic molecules with aromatic cores, we studied the effect of adding a chaotropic agent such as urea to the battery electrolyte to see if it improves the accessible concentration of active material and enhances the capacity utilization of the battery. Although reduction in aggregation was observed in NMR, this did not affect capacity utilization in the flow battery. Together, these studies provide a valuable understanding on how the structure of the redox-active molecules influence the electrochemical performance and stability of the flow battery.

KEYWORDS: electrochemistry, aqueous organic flow battery, organic molecules, naphthalene diimide, self-association

TURUN YLIOPISTO
Teknillinen Tiedekunta
Kone- ja materiaalitekniikan Laitos
Materiaalitekniikka
MAHSA SHAHSAVAN: Naftaleenidiimidiin Perustuvien Virtausakkujen Kehittäminen
Väitöskirja, 103 s.
Teknologian tohtoriohjelma
Kuukausi Vuosi

TIIVISTELMÄ

Siirtyminen uusiutuvien energialähteiden laajempaan hyödyntämiseen on välttämätöntä ilmastonmuutoksen hillitsemiseksi ja fossiilisiin polttoaineisiin liittyvän riippuvuuden vähentämiseksi. Aurinko- ja tuulienergian luontainen epäsäännöllisyys kuitenkin edellyttää tehokkaampien ja skaalautuvien energiavarastointijärjestelmien kehittämistä, jotta energiantuotanto ja -kulutus voidaan tasapainottaa luotettavasti. Virtausakut, erityisesti vesipohjaiset orgaaniset virtausakut, ovat nousseet lupaavaksi ratkaisuksi paikallaan pysyvään energian varastointiin niiden turvallisuuden sekä erityisesti niiden toisistaan riippumattoman tehon ja energian skaalattavuudenansiosta. Toisin kuin perinteisissä vanadiinipohjaisissa järjestelmissä, vesipohjaisissa orgaanisissa virtausakuissa hyödynnetään sähkökemiallisesti aktiivisia orgaanisia molekyylejä, jotka ovat houkuttelevia synteettisen muokattavuutensa ansiosta. Näiden molekyylien valmistamiseen ei tarvita harvinaisia materiaaleja, mikä saattaa mahdollistaa alhaiset tuotantokustannukset. Tässä väitöskirjassa lähestyimme vesipohjaisten orgaanisten virtausakkujen-kehitystyötä kahdesta suunnasta. Ensinnäkin tutkimme kahden uuden funktionalisoidun naftaleenidiimidin sähkökemiallisia ominaisuuksia ja suorituskykyä virtausakussa keskittyen niiden liukoisuuteen, sähkökemialliseen käyttäytymiseen ja kemialliseen stabiilisuuteen. Toiseksi, tutkimme kaotrooppisten aineiden kuten urean vaikutusta aromaattisten orgaanisten molekyylien kasautumiseen vesiliuoksissa. Tavoitteena oli ymmärtää, voidaanko kasautumista vähentämällä vaikuttaa akun kapasiteettiin. Vaikka urean lisäys vähensi molekyylien kasautumista, akun kapasiteetti ei muuttunut. Yhdessä nämä tutkimukset syventävät ymmärrystä siitä, miten hapetus-pelkistys-aktiivisten molekyylien rakenne vaikuttaa virtausakun sähkökemialliseen suorituskykyyn ja stabiilisuuteen.

ASIASANAT: vesipohjainen orgaaninen virtausakku, sähkökemia, orgaaniset molekyylit, naftaleenidiimidi, kasautuminen

Table of Contents

Abbreviations

ESS	energy storage system
VFB	vanadium flow battery
OFB	organic flow battery
AOFB	aqueous organic flow battery
RAOM	redox-active organic molecule
AEM	anion exchange membrane
CEM	cation exchange membrane
CE	coulombic efficiency
VE	voltage efficiency
EE	energy efficiency
CU	capacity utilization
SOC	state of charge
SHE	standard hydrogen electrode
Ag/AgCl	silver/silver chloride electrode
NMR	nuclear magnetic resonance spectroscopy
CV	cyclic voltammetry
RDE	rotating disk electrode
pH	potential hydrogen
CC	constant current
AQDS	9,10-anthraquinone-2,7-disulfonic acid
KCl	potassium chloride
NaCl	sodium chloride
NH_4Cl	ammonium chloride
$Na_4[Fe(CN)_6]$	sodium ferrocyanide
$K_4[Fe(CN)_6]$	potassium ferrocyanide
$(NH4)_4[Fe(CN)_6]$	ammonium ferrocyanide
NDI	naphthalene diimide
B-NDI	N, N′-bis(glycinyl) NDI
GABA-NDI	γ-aminobutyric acid functionalized NDI
ASP-NDI	aspartic acid functionalized NDI

List of Original Publications

This dissertation is based on the following original publications, which are referred to in the text by their Roman numerals:

I **Mahsa Shahsavan**, Cedrik Wiberg, Pekka Peljo. Gamma-aminobutyric acid-functionalized naphthalene diimide for aqueous organic flow batteries. *Chemical Communications*, 2022; **58**(64): 9052–9055.

II **Mahsa Shahsavan**, Cedrik Wiberg, Aapo Poskela, Johan Hjelm, Pekka Peljo. Demonstrating the performance of aspartic-acid functionalized naphthalene diimide in a near-neutral flow battery. Submitted.

III **Mahsa Shahsavan**, Cedrik Wiberg, Aapo Poskela, Pekka Peljo. Effect of urea as a chaotropic agent on self-association of organic molecules in aqueous flow batteries. Submitted.

Contribution Statement

Doctoral candidate's role in Publication I-III:

- Research design: Participated in conceptualization and methodology design.
- Laboratory work: Conducted investigations and experimental work.
- Data processing: Performed formal analysis, validation, and visualization of results.
- Writing of the manuscript: Wrote the original draft and contributed to review and editing.
- Article is/will be used in multiple doctoral thesis: No.

1 Introduction

The urgent need to reduce carbon emissions and to limit the effects of global warming has resulted in a shift toward using more renewable energy resources such as solar and wind. However, these resources suffer from intermittent availability so as shown in Figure 1, it essential to develop efficient and scalable energy storage systems (ESSs) to connect the gap between energy production and energy consumption. [1]

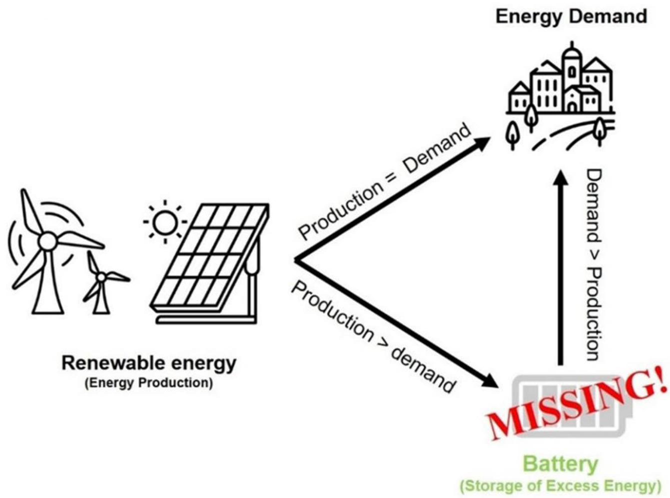

Figure 1. Scheme showing the importance of ESSs.

Among all ESSs, flow batteries have emerged as a promising solution for medium to large-scale stationary energy storage. The advantages of flow batteries including long cycle life, independent scaling of power and energy and the enhanced safety make them ideal for integrating renewables efficiently into the grid. While vanadium flow batteries (VFBs) are the most established system on the commercial scale, their cost and dependency on limited vanadium resources have led the researchers to look for alternative chemistries for flow batteries. [2,3]

In recent years, aqueous organic flow batteries (AOFBs) have gained attention due to the tunability, the prospects of low cost and sustainability of organic molecules. The use of redox-active organic molecules (RAOMs) in flow batteries allows the properties such as redox potential, solubility and chemical stability to be tailored through functional group modifications and therefore offer an opportunity for designing more efficient flow batteries. [4]

In this thesis, we investigated the development of AOFBs by taking two research directions. First, the electrochemical behaviour and flow battery performance of two newly functionalized naphthalene diimides (NDIs) were studied in the flow battery (**Publication I and II**). Second, to address the self-association behaviour of RAOMs with aromatic core, we investigated whether the addition of a chaotropic agent such as urea could reduce or prevent self-association and therefore improving the flow battery performance (**Publication III**). These studies deepen the understanding of structure-related properties of RAOMs on the flow battery performance and provide insight into the design of more efficient flow battery systems.

2 Flow Batteries

2.1 Operating Principle of Flow Batteries

A flow battery operates by circulating electrolytes that contain redox-active molecules through electrochemical cell(s) in which energy conversion takes place. §Unlike conventional batteries such as lithium-ion batteries where the energy storage and energy conversion happen within solid electrodes, flow battery decouples power and energy. This means that the energy is stored separately in electrolyte tanks and the power is determined by the size and number of electrochemical cells. This separation enables independent scaling of energy and power and is beneficial for grid-level applications and increases the safety of the storage system. Electrochemical reactions in flow battery involves simultaneous oxidation and reduction reactions at two different electrodes. During charge and discharge, electrolyte solutions containing oxidized and reduced forms of redox couples are pumped from external storage tanks into the electrochemical cell(s). The electrochemical cell typically consists of two half-cells separated by an ion-selective membrane that permits ion transfer to maintain charge balance while preventing crossover of redox species (**Figure 2**). [5]

Flow batteries offer several advantages over conventional batteries such as:

- Scalability: Energy (determined by the size of the tanks) and power (determined by the size and number of electrochemical cells) can be scaled independently. This means that increasing the tank size increases the energy storage capacity while bigger cells or adding more cells increases the power output.
- Safety: Aqueous systems are non-flammable.
- Long cycle life: Electrodes in flow batteries do not undergo structural changes like solid electrodes. This feature along with the reversible redox reactions results in thousands of charge and discharge cycles. [6,7]

Despite being promising, AOFBs face several challenges that has so far hindered their large-scale commercial integration such as:

- Low energy density: Most of the RAOMs have limited solubility in water that lowers the energy density of the flow battery. [8,9]

- Molecular stability: One of the most critical issues in AOFBs is the chemical and electrochemical stability of the RAOMs. RAOMs can undergo decomposition through hydrolysis, oxidation or other side reactions under operating conditions that results in capacity fade and decreases the lifetime of the flow battery. [10,11]
- Membrane crossover: Some of the RAOMs can permeate through ion-exchange membranes. This leads to cross-contamination, reduced efficiency and the need for frequent rebalancing of the electrolytes. [12]
- Synthetic and economic viability: While one of the main advantages of RAOMs is their structural tunability, many promising candidates are still synthetically complex or expensive to produce at large scale. [13]
- Osmosis: Due to the differences in osmotic pressure between the electrolyte tanks, water molecules permeate through the membrane. This results in electrolyte volume imbalance and therefore causes overflow or depletion in one tank or the other and changes the concentration of the redox-active species. [6]
- Self-association: RAOMs with aromatic cores such as quinones and NDIs often undergo π–π stacking in aqueous environments that leads to self-association. [14,15] This phenomenon will be discussed in chapter 4.

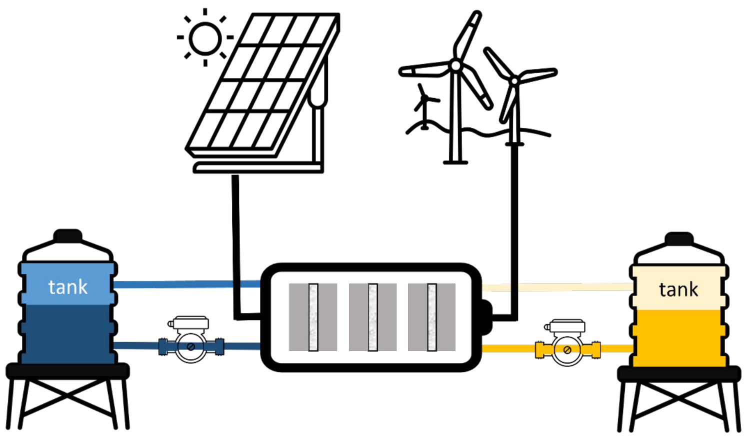

Figure 2. Simplified scheme of a flow battery.

2.2 Different Types of Flow Batteries

A wide variety of flow battery chemistries have been investigated in the recent decades. In general, flow batteries can be grouped according to the nature of the redox-active species and the electrolyte medium. The main groups are:

- Vanadium flow batteries (VFBs)
- Aqueous inorganic systems such as iron-chromium ($Fe^{2+}/Fe^{3+} \| Cr^{2+}/Cr^{3+}$) and hydrogen-bromine.
- Hybrid systems such as zinc-bromine, zinc-iodine, or zinc-nickel.
- Organic flow batteries (OFBs) with RAOMs as active species that can be aqueous (AOFBs) or non-aqueous depending on the solvent.
- Membrane-free systems such as laminar- and immiscible-phase flow batteries.
- Solid-mediated and semi-solid flow batteries that incorporate solid electroactive materials either as suspensions or stored externally.
- Emerging concepts including solar flow batteries and metal-air flow systems.

Among these systems, two classes have attracted particular attention for large-scale energy storage: VFBs which have been the most extensively investigated and OFBs due to their potential for cost reduction and molecular tunability. The following discussion therefore focuses on these two families. [16]

A VFB employs vanadium ions in different oxidation states (V^{2+}/V^{3+} and VO^{2+}/VO_2^{+}) as redox-active species. However, the widespread implementation of VFBs is limited by factors such as the high cost and supply limitations of vanadium. These factors have diverted the research direction to look for alternative chemistries. [3]

In the pursuit of alternative chemistries, RAOMs have emerged as promising candidates for flow batteries. Organic molecules can be synthetically modified to tune the properties such as redox potential, solubility and stability. [17] Based on the solvent used in the electrolyte, OFBs can be categorized into aqueous and non-aqueous. Non-aqueous organic flow batteries have a wider electrochemical stability window that can theoretically lead to higher cell voltages and energy densities; however, they face several critical challenges such as the use of expensive, toxic and flammable solvents with lower ionic conductivity compared to the aqueous systems. These drawbacks limit the practical applicability of non-aqueous flow batteries especially for large-scale storage. [18] Taking all of these concerns into account, AOFBs have gained more attention among researchers. Water-based electrolytes in AOFBs are non-flammable, inexpensive and provide high ionic conductivity that makes them more suited for large-scale storage. Nevertheless, AOFBs still face challenges related to molecular stability, solubility limits and phenomena like self-association or irreversible degradation of the organic molecules. [8,19]

2.3 Recent Progress in Aqueous Organic Flow Batteries

Progress in organic synthesis and molecular engineering have resulted in the development of RAOMs specifically tailored for AOFBs. These developments have focused on enhancing aqueous solubility, enabling multi-electron transfer and improving chemical and electrochemical stability under mostly neutral conditions. [8,13] One major strategy in molecular engineering involves adding functional groups to enhance solubility and tune redox potentials. Hydrophilic substituents such as sulfonate, carboxylate or phosphonate groups are often introduced to improve solubility while electron-donating or electron-withdrawing moieties can change redox potentials. [20,21] Using these strategies, different organic molecules have been explored for both the positive and negative electrolytes in flow batteries. Since the focus of this thesis is on the development of negative electrolyte materials, only some of candidates designed for the negative electrolyte in the flow battery will be discussed. In this context the most studied molecules are quinones and viologens.[12,22–24] Recently, naphthalene diimides (NDIs) have received attention for their reversible redox behavior, molecular tunability and have demonstrated promising performance in flow batteries operating under near-neutral conditions. [15,25]

2.3.1 Quinones

Quinone derivatives have gained attention in flow batteries due to their fast redox kinetics and synthetic tunability. The examples discussed in this section are not intended to be comprehensive of all quinone-based electrolytes reported in the literature. Instead, we only discuss the systematic work of the research group led by Prof. Aziz at Harvard University which has been at the forefront of developing and optimizing quinone-based molecules for AOFBs.

The foundational work on quinones began in 2014 with the introduction of 9,10-anthraquinone-2,7-disulfonic acid (AQDS) as a RAOM in flow batteries. Paired with bromine, this system demonstrated high capacity retention over 100 cycles and therefore establishing AQDS as a reference molecule for the upcoming designs. [26]

In 2016, the group investigated a broader set of anthraquinone derivatives, including anthraquinone-2-sulfonic acid (AQS), 1,8-dihydroxyanthraquinone-2,7-disulfonic acid (DHAQDS), 1,4-dihydroxyanthraquinone2,3-dimethylsulfonic acid (DHAQDMS) and alizarin red S (ARS) for their compatibility in flow batteries with bromine. While molecules like DHAQDS and ARS showed low redox potentials, they underwent undesirable side reactions with bromine. DHAQDMS was compatible with bromine but showed irreversible reduction. In contrast, AQS displayed both redox stability and bromine compatibility therefore making it a strong candidate for bromine-based flow batteries. [21]

In 2018, the group introduced an ether-functionalized anthraquinone, 4,4'-((9,10-anthraquinone-2,6-diyl) dioxy) dibutyrate (2,6-DBEAQ), which demonstrated significantly improved aqueous solubility and excellent cycling stability when paired with a ferro/ferricyanide. This system exhibited a capacity fade rate of less than 0.01% per day. [10] In the same year, the group developed a benzoquinone-based flow batteries using 2,5-dihydroxy-1,4-benzoquinone (DHBQ) that showed promising results in alkaline flow batteries. [27]

Building on these studies in 2019, a phosphonate-functionalized anthraquinone, ((9,10-dioxo-9,10-dihydroanthracene-2,6-diyl) bis(oxy)) bis (propane-3,1 diyl)) bis (phosphonic acid) (2,6-DPPEAQ) was synthesized. This molecule achieved a record-low capacity fade rate of 0.014% per cycle in near neutral pH conditions. [28] In the same year, 2,2′-bis (3- hydroxy-1,4-naphthoquinone) (bislawsone) was introduced that is a dimerized naphthoquinone structure. Bislawsone outperformed its monomeric counterpart in terms of solubility and voltage and showed performance improvements under alkaline conditions with capacity fade rate of 0.75% per day. [29]

In 2020, 3,3′-(9,10-Anthraquinone-diyl) bis (3-methylbutanoic acid) (DPivOHAQ) and 4,4′-(9,10-anthraquinone-diyl) dibutanoic acid (DBAQ) were synthesized from inexpensive 9,10-dihydroanthracene precursors. These derivatives demonstrated excellent stability with capacity fade rates of 0.014% and 0.0084% per day, respectively. [30]

In 2022, the group reported sodium 3,3′,3″,3‴-((9,10-anthraquinone-2,6 diyl) bis(azanetriyl)) tetrakis(propane-1-sulfonate) (2,6-N-TSAQ), a three sulfonated anthraquinone derivative. Although stable at high pH, this molecule exhibited poor cycling stability at neutral pH due to increased anthrone formation. [31] Later that year, they developed 2-2-propionate ether anthraquinone (2-2PEAQ) that showed capacity fade rates of 0.03-0.05% per day at neutral pH. [24]

In 2023, 2,2′((9,10-dioxo-9,10-dihydroanthracene-2,6-diyl) bis(oxy)) dipropionic acid (2,6-D2PEAQ), a chiral anthraquinone derivative featuring a methyl-branched, carboxylate-terminated ether side chain was introduced which is a double substituted variant of 2-2PEAQ. This molecule has solubility up to 2 M at pH 7. It demonstrated outstanding cycling stability in the same pH with the capacity fade rate of 0.02% per day lower than the monosubstituted molecule. [23]

Finally, the group designed 3-NH_2-2-2PEAQ which includes both ether and amino substituents to suppress decomposition. This molecule exhibited high solubility of 1 M at pH 14 and a fade rate of 0.01% per day. [32]

Overall, the work of the Aziz group has significantly advanced the development of quinone-based electrolytes for AOFBs. Through systematic molecular engineering including substitutions with sulfonate, ether, phosphonate, and carboxylate groups, they have demonstrated how tuning redox-active cores can enhance solubility, stability and electrochemical performance across different pH conditions. For instance, sulfonate groups increase water solubility and chemical stability in acidic and neutral media by enhancing hydrophilicity and charge delocalization. Ether substituents improve aqueous solubility and suppress aggregation without significantly affecting redox potential. Phosphonate groups stabilize the reduced state and slow capacity fade under near-neutral conditions through strong electron-withdrawing effects and hydrogen-bonding interactions. Carboxylate group improve solubility and long-term stability in neutral electrolytes, while causing a modest negative shift in redox potential due to its weak electron-donating character. Representative examples of quinone molecules developed in Aziz group are shown in Figure 3.

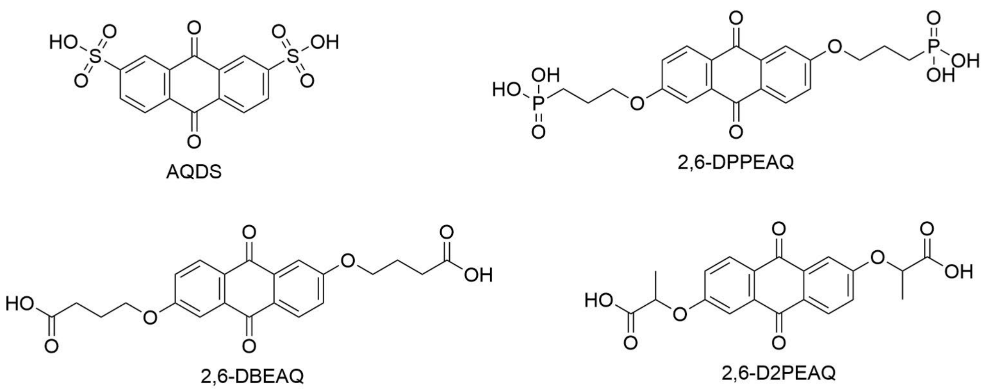

Figure 3. Structure of quinone derivatives including AQDS, [26] 2,6-DPPEAQ, [29] 2,6-DBEAQ [27] and 2,6-D2PEAQ [23] with different functionalization (sulfonate, phosphonate, ether, and carboxylate).

2.3.2 Viologens

Viologen derivatives are another studied families of RAOMs in the context of AOFB. In this section, only a subset of reported viologen derivatives is discussed to illustrate how different functionalization influence solubility, stability and cycling behaviour of this family.

In 2016 a flow battery employing methyl viologen (MV) paired with 4-hydroxy-2,2,6,6-tetramethylpiperidinoxyl (4-OH-TEMPO) was studied. However, the full reduction of MV is hindered by the insolubility of the charge-neutral MV species. [33] In addition, later studies have identified issues such as MV dimerization, membrane crossover and other stability challenges that affect long-term cycling performance of MV in flow batteries. [34,35]

In 2017, 1-methyl-1′-[3-(trimethylammonio) propyl]-4,4′-bipyridinium trichloride ([(Me)(NPr)V] Cl_3) and 1,1′-bis[3-(trimethylammonio) propyl]-4,4′-bipyridinium tetrabromide ([$(NPr)_2$V] Br_4) was developed by the same group that reported the MV-based flow batteries in 2016 through functionalization of 4,4'-bipyridine with hydrophilic substituents. These two derivatives are capable of undergoing two-electron reductions and exhibited enhanced durability under neutral pH. [36] In the same year, bis(3-trimethylammonio) propyl viologen tetrachloride (BTMAP-Vi) was introduced by Aziz group as a highly soluble and cationic derivative that addressed the solubility and crossover limitations of MV. The incorporation of quaternary ammonium side chains enhanced aqueous compatibility and reduced dimerization through steric and electrostatic effects and enabled stable cycling at neutral pH when paired with ferro/ferricyanide. [37]

By 2018, a sulfonate-functionalized viologen derivative namely 1,1′-bis(3-sulfonatopropyl)-4,4′bipyridinium ($(SPr)_2V$), was introduced to improve aqueous solubility and stability under neutral pH conditions. While $(SPr)_2V$ demonstrated enhanced stability compared to earlier viologens, it still exhibited rapid capacity fade related to the neutral character of its oxidized form that promoted crossover and decreased retention during long-term cycling. [12]

In 2020, Aziz group introduced a phosphonate-functionalized viologen derivative 1,1′-bis(3-phosphonopropyl)- [4,4′- bipyridine]-1,1′-diium dibromide (BPP−Vi) operating at near-neutral pH. BPP-Vi exhibited exceptionally low membrane permeability and improved long-term capacity retentio while maintaining a low redox potential. [22]

In 2021, rod-shaped sulfonated viologen (R-Vi) was synthesized to suppress side reactions and dimerization through steric hindrance at the bipyridine core. This design yielded improved stability and led to long-duration cycling with minimal capacity fade. [38]

In 2022, π-conjugation-extended bipyridinium derivatives (exBPs) was designed that enabled reversible two-electron reductions at neutral pH and therefore doubling the energy density of viologen-based AOFBs. [39]

In 2023, PEGylated viologen (BTMAE-Vi) was developed that incorporates positively charged ethylene glycol side chains with solubility of up to 3.4 M and suppresses crossover in neutral-pH flow batteries but is prone to decomposition in the fully reduced state. [40]

Most recently in 2025, 1-methyl-1′-(3-sulfonate) propyl-4,4′-bipyridinium iodide (MSPVI) was introduced for neutral pH electrolytes. The asymmetrical substitution in this molecule not only enhanced solubility but also introduced steric and electrostatic effects that disrupted the efficient π-π stacking of reduced viologen radicals, therefore, mitigated the dimerization compared to MV. [41]

Overall, viologen derivatives have advanced from the simple MV system that was limited by poor solubility, dimerization and crossover to a wide range of molecules designed for improved performance. For example, quaternary ammonium substituents as in BTMAP-Vi increase aqueous solubility, suppress dimerization, and reduce membrane crossover through steric and electrostatic repulsion. Sulfonate groups enhance hydrophilicity and compatibility at neutral pH but when present in symmetric structures, can promote crossover of the neutral form. Phosphonate groups strongly decrease membrane permeability and improve long-term stability under near-neutral conditions owing to their electron-withdrawing and hydrogen-bonding characteristics. Bulky or rod-shaped architectures further stabilize the reduced species by hindering π–π stacking and aggregation at the bipyridinium core. Representative examples of viologen molecules are shown in Figure 4.

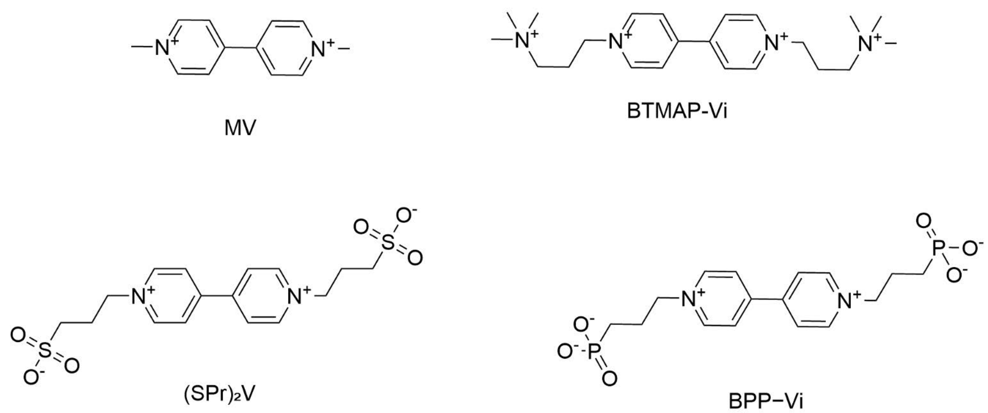

Figure 4. Structure of viologen derivatives including MV, [33] BTMAP-Vi (bis(trimethyl ammonium propyl) functionalized), [37] $(SPr)_2V$ (sulfonate-functionalized) [12] and BPP-Vi (phosphonate-functionalized). [22]

2.3.3 Naphthalene Diimides

Naphthalene diimides (NDIs) consist of a naphthalene backbone with two imide functionalities and resemble quinones in both their molecular structure and their redox behaviour. Water soluble NDIs undergo reversible two electron reduction processes; however, NDIs are prone to self-association through π-π stacking interactions of their aromatic core. [15] The electrochemical behaviour of NDIs can be tuned by introducing substituents on the naphthalene core, while the choice of side chains at the imide positions influences aqueous solubility and can suppress self-association. [42] In NDIs, reduction occurs at the conjugated aromatic core. The first reduction leads to a radical anion ($NDI^{\bullet-}$) followed by the second reduction to form the dianion (NDI^{2-}). The redox potentials of these reductions are typically well separated therefore giving rise to two distinct redox couples as shown in Figure 5. Although some molecular designs have merged these two redox couples into a one-step two-electron process so that both reductions happen in the same potential. [43]

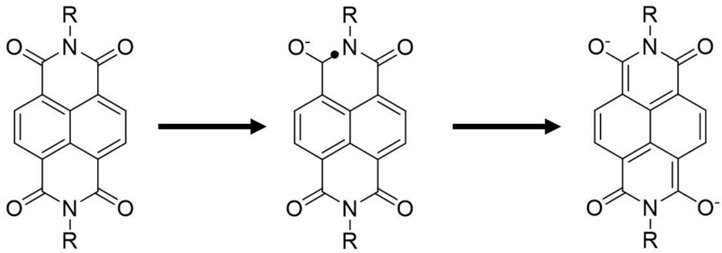

Figure 5. Stepwise reduction of NDIs from charge neutral to radical anion ($NDI^{\bullet-}$) and to dianion (NDI^{2-}).

The exploration of NDIs as redox-active molecules for flow batteries began with electrochemical evaluations done by Wiberg *et al*. in 2019 on a quaternary amine-functionalized naphthalene diimide (D-NDI). D-NDI has a solubility of 0.68 M in water and undergoes a reversible two separate electron redox processes. However, NMR measurements at different concentrations of D-NDI revealed pronounced self-association of the molecules at higher concentrations. [15]

In 2020, Medabalmi *et al*. demonstrated the first NDI-based flow battery with N, N′-bis(glycinyl) naphthalene diimide (B-NDI) that is synthesized through the introduction of carboxylate substituents on the imide nitrogens. The aqueous solubility of its potassium and sodium salts reached 167 mM and 210 mM in water, respectively, but decreased to 30 mM in 1 M potassium chloride (KCl) and 40 mM in 1 M sodium chloride (NaCl). When dissolved, B-NDI carries negative charges and was paired with 4-OH-TEMPO across an anion-exchange membrane (AEM) in neutral pH conditions but the crossover of 4-OH-TEMPO through the AEM caused rapid capacity fade in this study. However, no molecular decomposition of NDIs was detected after cycling indicating that the capacity loss is not due to the instability of the B-NDI. [44]

In 2021, Wiberg *et al*. reported two types of NDI molecules: a core-unsubstituted derivative, N, N′-bis(dimethylaminopropyl)-NDI (2H-NDI) and a core-dimethylamino substituted analogue, N, N′-bis(dimethylaminopropyl)-2,6-bis(dimethylamino)-NDI (2DMA-NDI). These molecules were paired with bis((3-trimethylammonio) propyl) ferrocene dichloride (BTMAP-Fc) across an AEM in neutral pH. In this study, the choice of supporting electrolyte had a pronounced impact on cycling behaviour. In the case of 2H-NDI with potassium-based electrolytes, the cells exhibited gradual capacity fade which was related to the formation of electrochemically inactive species. In contrast when ammonium-based electrolytes were used, a slow increase in capacity was observed but at the expense of lower energy efficiencies (EE). While the exact mechanism was not fully described, the difference between the two systems was concluded to be the ability of ammonium cations to more effectively shield the negative charges on the reduced NDI species and therefore suppressing the formation of inactive species during the cycling. Flow batteries employing this NDI at higher concentrations in ammonium-based electrolytes exhibited more rapid capacity decay compared to lower concentrations. This fading was attributed mainly to BTMAP-Fc crossover through the AEM and this effect was made worse because at high concentration, 2H-NDI tends to self-associate more which slows down its transport to the electrode and limits the accessible capacity. Importantly, the active material itself remained chemically stable during cycling. Unlike 2H-NDI, 2DMA-NDI undergoes a two-electron and two-proton reduction at neutral pH. Its capacity fade was lower than that of 2H-NDI with the main causes identified as BTMAP-Fc crossover and partial decomposition of 2DMA-NDI in potassium-based electrolytes. When potassium was replaced with ammonium, the flow battery instead displayed a gradual capacity increase during the initial cycles and showed no measurable capacity fade over extended cycling. [25]

In 2022 and as described in **Publication I**, we introduced γ-aminobutyric acid (GABA) functionalization to the NDI that introduces negative charges similary to B-NDI and with enhanced aqueous solubility. The findings from this study will be presented in details in chapter 4. [19]

In the same year, Singh *et al.* introduced a di-ammonium-functionalized NDI (A^{2+}-Et-NDI) with an aqueous solubility of 0.7 M in water and 0.5 M in 1.5 M KCl. The enhanced solubility was attributed to the incorporation of highly soluble di-ammonium substituents. Positively charged A^{2+}-Et-NDI was employed with a cation-exchange membrane (CEM) in a flow battery using iodide/triiodide redox couple. The system exhibited a capacity fade of 0.0026% per cycle (0.075% per day). Post-mortem analysis revealed negligible chemical decomposition of the active species. However, crossover of iodide/triiodide into the NDI side was detected. Further experiments showed that the permeability of iodide/triiodide through the membrane was approximately 30 times higher than that of the NDI species. Considering the 3.3-fold volume ratio between the positive and negative electrolytes, this imbalance leads to gradual charge mismatch between the two sides and consequently to capacity fade. [45]

In 2023, Pan *et al.* reported two quaternary ammonium-functionalized naphthalene diimides: bis-[(3-trimethylamino) propyl] NDI dichloride ([A-NDI] Cl_2) with solubilities of 1.0 M in water and 0.87 M in 1 M NaCl, and bis(3-(bis(2-hydroxyethyl) methylamino) propyl) NDI dichloride ([HA-NDI] Cl_2) with lower solubilities of 0.78 M in water and 0.58 M in 1 M NaCl. These results indicated that the introduction of hydroxyethyl substituents does not enhance the solubility of NDIs. When paired with N^{Me}-TEMPO across an AEM, [A-NDI] Cl_2/N^{Me}-TEMPO flow battery achieved fade rate of 0.0023% per cycle (0.094% per day), while [HA-NDI] Cl_2/N^{Me}-TEMPO flow battery showed a slightly higher fade rate of 0.00394% per cycle (0.229% per day). In both cases, crossover into the NDI side and partial decomposition of TEMPO were identified as the main contributors of capacity loss. [46]

In the same year, Singh *et al*. developed tetra-ammonium-functionalized NDI ($4A^{4+}$-NDI) derivatives with high solubilities of 1.5 M in water and 1.2 M in 1.5 M KCl. When tested in a flow battery paired with the iodide/triiodide redox couple over a CEM, a capacity fade of 0.004% per cycle (0.044% per day) was obtained and it was attributed primarily to minor physical effects such as temperature fluctuations, membrane resistance variations and accidental touching of the tanks. [47] However, as in their previous work, a small degree of iodide/triiodide crossover into the NDI side was also detected. [45]

In 2024, Wang *et al*. introduced two core-substituted NDIs namely N, N′-bis((trimethylamino)propylamino)-2,6-bis(dimethylamino)-1,4,5,8 naphthalene tetracarboxylic dianhydride dichloride (NDI-DMe) and N, N′-bis((trimethylamino) propylamino)-2,6-bis ((2-hydroxyethyl) amino)-4,5,8-naphthalenetetracarboxylic dianhydride dichloride (NDI-DEtOH) that are designed to undergo one-step two-electron transfer. The introduction of electron-donating substituents at the NDI core increases electron density of the π-conjugated aromatic backbone of NDI and helps with the charge delocalization and therefore reduces the Coulombic repulsion. This leads to merging the two sequential reductions into a single two-electron process. The one-step two-electron transfer is advantageous for flow batteries eliminates the formation of unstable radical intermediates. NDI-DMe exhibited solubilities of 0.92 M in water and 0.61 M in 2 M NaCl, while NDI-DEtOH reached the solubility of 0.94 M in water and 0.65 M in 2 M NaCl due to the greater hydrophilicity of the hydroxyethyl groups. Compared to the core unsubstituted D-NDI, however, the solubilities of these derivatives were lower due to the increased molecular volume introduced by the substitution. Flow battery employing an AEM with (ferrocenylmethyl)trimethylammonium chloride (FcNCl) showed capacity fade rates of 0.045% per cycle (4.5% per day) for NDI-DEtOH compared to 0.07% per cycle (7.5% per day) for NDI-DMe. In this study, capacity fade was attributed to FcNCl crossover and partial hydrolysis of the imide groups. The latter was confirmed by NMR and was linked to the pH change in the electrolyte during cycling. [43]

In the same year, Liu *et al*. synthesized a series of NDI derivatives such as siol-NDI, diol-NDI, and dex-NDI via a hydrothermal method with solubilities of 1.60, 1.85, and 2.13 M in water, respectively. The enhanced solubility of these derivatives was attributed to the introduction of hydroxyl groups and positively charged quaternary ammonium salts. Among these, dex-NDI emerged as the most promising candidate. When paired with MiAcNH-TEMPO in a flow battery using an AEM, a fade rate of 0.0052% per cycle (0.114% per day) was achieved. The observed capacity fade was mainly linked to water permeation through the membrane which increased electrolyte viscosity and internal resistance. [48]

In 2025, H. Zhang *et al*. synthesized zwitterionic NDI derivatives ($(SPr)_2NDI$, $(SPrOH)_2NDI$, and $(CBu)_2NDI$) via an atmospheric pressure heating method. Their solubilities were 0.69 M in water (0.33 M in 1 M NaCl) for $(SPr)_2NDI$, 0.31 M in water for $(SPrOH)_2NDI$, and 1.49 M in water (1.32 M in 1 M NaCl) for $(CBu)_2NDI$. The higher solubility of $(CBu)_2NDI$ was attributed to the presence of more charge centers in the molecule. All three derivatives displayed two step-wise one electron reduction processes. Flow batteries pairing $(SPr)_2NDI$ or $(CBu)_2NDI$ with potassium ferrocyanide ($K_4Fe(CN)_6$) across a CEM at neutral pH exhibited excellent cycling stability with no measurable capacity fade per cycle even at high concentrations with no evidence of crossover. However, post-mortem NMR analysis revealed slight decomposition of the NDI molecules after extended cycling. [49]

In the same year, X. Zhang *et al*. introduced imidazolium-functionalized NDIs (NDI-C_2-MzMe, NDI-C_3-MzMe, and NDI-C_3-MzOH) via a multi-hydrogen-bond engineering strategy. These molecules showed high solubilities of 0.59, 1.26, and 1.43 M in water (and 0.42, 1.07, and 1.26 M in 1 M NaCl), respectively. The solubility increases from C_2 to C_3 to C_3-OH was attributed to longer alkyl linkers and terminal hydroxyl groups. In flow battery with MiAcNH-TEMPO across an AEM, the concentration of 0.1 M of the NDIs exhibited fade rates of 0.0012% per cycle (0.2317% per day) for NDI-C_2-MzMe, 0.080% per cycle (1.29% per day) for NDI-C_3-MzMe, and 0.0039% per cycle (0.681% per day) for NDI-C_3-MzOH. At the concentration of 1 M, NDI-C_3-MzMe and NDI-C_3-MzOH showed capacity fade of 0.0437% per cycle (1.14% per day) and 0.0225% per cycle (0.488% per day), respectively. The observed capacity loss was mainly linked to a slight reversible hydrolysis of the imidazolium-NDIs during charge when the pH drifted to mildly alkaline values by creating small amounts of redox-inactive by-products. However, since this reaction is reversible and the electrolyte remains near-neutral the long-term stability was not much affected. [50]

Finally, in **Publication II**, we introduced an aspartic acid-functionalized NDI (ASP-NDI) which exhibited a solubility of 1.07 M in water. The detailed findings of this study will be discussed in chapter 4.

Overall, similar to the previously discussed redox-active families, functionalization of the NDIs with different substituents can change their chemical and electrochemical properties. Quaternary ammonium, zwitterionic, and imidazolium substituents increase solubility and suppress aggregation through electrostatic and steric effects, while carboxylate groups such as in B-NDI, GABA-

NDI, and ASP-NDI introduce anionic character and strong hydrophilicity that enhance solubility under neutral conditions. Core substitutions with electron-donating groups increase π-electron density and reduce Coulombic repulsion during reduction and merges the two sequential redox steps into a single two-electron process that improves energy efficiency. Despite these advances, capacity fade in some NDI-based flow batteries is influenced by membrane crossover, side reactions at high concentrations and in some cases the mechanisms behind capacity loss remain under debate. To conclude, NDIs represent a promising yet still emerging class of RAOMs where further progress in molecular design and better understanding of the system is required before NDIs can reach the stability and performance benchmarks established by more mature systems such as quinones. The structures of NDI derivatives developed for flow batteries are illustrated in Table 1.

Table 1. Evolution NDI derivatives employed in AORFBs from 2019 to 2025.

NAME (Year)	**STRUCTURE**	**SOLUBILITY (M)**	**REDOX POTENTIAL (V *vs.* SHE)**	**DIFFUSION COEFFICIENT $\times 10^{-6}$ (cm^2/s)**	**CAPACITY FADE RATE**
D-NDI [15] (2019)	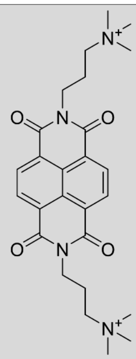	0.68 (water)	1^{st}: −0.21 2^{nd}: −0.63	-----	-----
B-NDI [44] (2020)	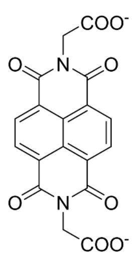	**K_2-B-NDI** 0.17 (water) 0.03 (1.0 M KCl) **Na_2-B-NDI** 0.21 (water) 0.04 (1.0 M NaCl)	1^{st}: −0.20 2^{nd}: −0.47	(1^{st}) 3.95 (2^{nd}) 1.95	0.1830% (per cycle) -----

2H-NDI [25] **(2021)**	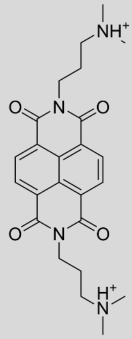	-----	1st: −0.28 2nd: −0.62	-----	-----
2DMA-NDI [25] **(2021)**	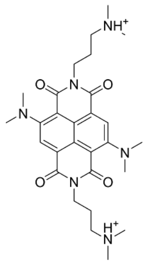	-----	1st & 2nd: −0.28	-----	-----
A^{2+}-ET-NDI [45] **(2022)**	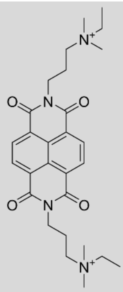	0.70 (water) 0.50 (1.5 M KCl)	1st: −0.24 2nd: −0.54	(1st) 3.09 (2nd) 1.97	0.0026% (per cycle) 0.0750% (per day)
GABA-NDI (PUBLICATION I, 2022) [19]	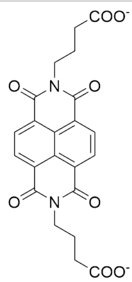	0.59 (water) 0.25 (1 M NH_4Cl)	1st: −0.12 2nd: −0.43	(average) 3.7	0.0213% (per cycle) 0.3600% (per day)

A-NDI [46] **(2023)**	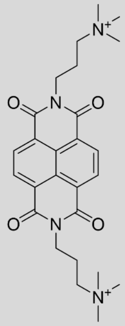	1.0 (water) 0.87 (1.0 M NaCl)	1^{st}: −0.018 2^{nd}: −0.456	(1^{st}) 4.02 (2^{nd}) 1.84	0.0023% (per cycle) 0.0940% (per day)
HA-NDI [46] **(2023)**	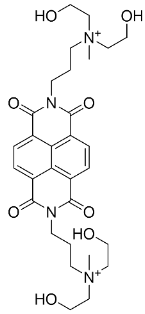	0.78 (water) 0.58 (1.0 M NaCl)	1^{st}: −0.024 2^{nd}: −0.450	(1^{st}) 2.97 (2^{nd}) 2.00	0.0039% (per cycle) 0.2290% (per day)
$4A^{4+}$-NDI [47] **(2023)**	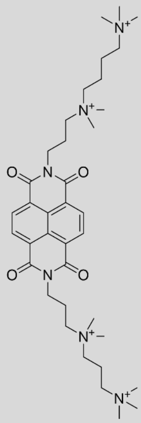	1.5 (water) 1.2 (1.5 M KCl)	1^{st}: −0.21 2^{nd}: −0.50	(1^{st}) 2.38 (2^{nd}) 1.42	0.0040% (per cycle) 0.0440% (per day)
NDI-DME [43] **(2024)**	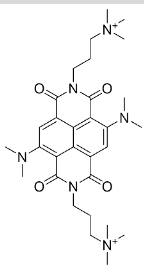	0.92 (water) 0.61 (2.0 M NaCl)	1^{st} & 2^{nd}: −0.41	3.63	0.0450% (per cycle) 4.5000% (per day)

NDI-DETOH [43] (2024)	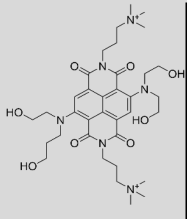	0.94 (water) 0.65 (2.0 M NaCl)	1st & 2nd: −0.37	4.46	0.0700% (per cycle) 7.5000% (per day)
SIOL-NDI [48] (2024)	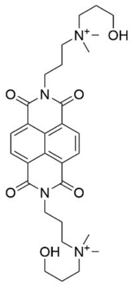	1.6 (water)	1st: −0.08 2nd: −0.44	(1st) 2.55 (2nd) 2.5	0.0244% (per cycle)
DIOL-NDI [48] (2024)	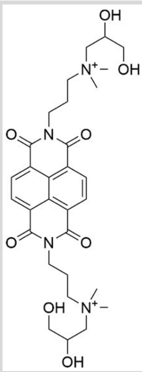	1.85 (water)	1st: −0.09 1st:−0.45	(1st) 5.7 (2nd) 2.43	0.0388% (per cycle)
DEX-NDI [48] (2024)	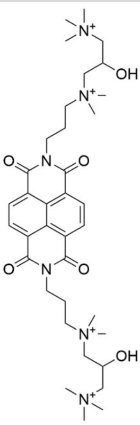	2.13 (water)	1st: −0.09 2nd: −0.42	(1st) 3.04 (2nd) 1.52	0.0052% (per cycle) 0.1141% (per day)

$(SPR)_2NDI$ [49] (2025)	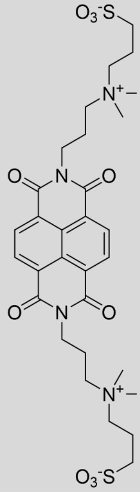	0.69 (water) 0.33 (1.0 M NaCl)	1st: −0.11 2nd: −0.43	(1st) 1.62 (2nd) 4.5	0%
$(SPROH)_2NDI$ [49] (2025)	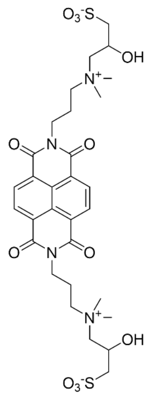	0.31 (water)	1st: −0.11 2nd: −0.44	(1st) 3.7 (2nd) 2.09	-----
$(CBU)_2NDI$ [49] (2025)	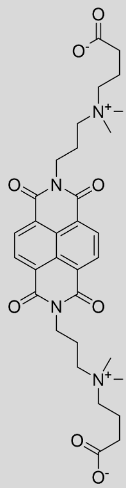	1.49 (water) 1.32 (1.0 M NaCl)	1st: −0.11 2nd: −0.44	(1st) 3.54 (2nd) 1.35	0%

NDI-C_2-MZME [50] (2025)	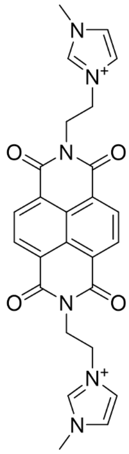	0.59 (water) 0.42 (1.0 M NaCl)	1^{st}: −0.07 2^{nd}: −0.44	(1^{st}) 3.05 (2^{nd}) 1.91	0.0800% (per cycle) 1.2900% (per day)
NDI-C_3-MZME [50] (2025)	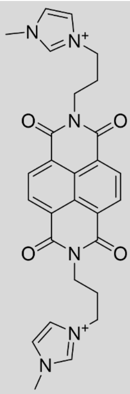	1.26 (water) 1.07 (1.0 M NaCl)	1^{st}: −0.09 2^{nd}: −0.44	(1^{st}) 5.99 (2^{nd}) 3.44	0.0437% (per cycle) 1.1400% (per day)
NDI-C_3-MZOH [50] (2025)	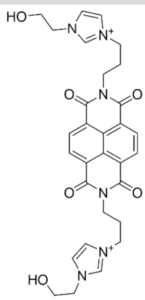	1.43 (water) 1.26 (1.0 M NaCl)	1^{st}: −0.08 2^{nd}: −0.44	(1^{st}) 1.01 (2^{nd}) 1.69	0.0225% (per cycle) 0.488% (per day)
ASP-NDI (PUBLICATION II, 2025)	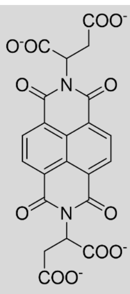	1.07 (water) 0.7 (1.0 M NH_4Cl)	1^{st}: −0.3 2^{nd}: −0.42	3.61	0.0104% (per cycle) 0.0275% (per day)

2.4 Self-association of Redox-Active Organic Molecules

As mentioned before, one of the challenges in AORFBs is the self-association of RAOMs such as quinone, viologen and NDIs.

Quinones such as AQDS undergo concentration-dependent dimerization and quinhydrone formation. In 2017, Carney *et al*. showed that above 10 mM, AQDS reversibly dimerizes that leads to a drop in accessible capacity from 2 to 1-1.5 electrons per molecule. [51] Later, Wiberg *et al.* quantified equilibrium constants of 5 M^{-1} in acidic media and 8 M^{-1} in alkaline media and demonstrated that the dimer is electrochemically inactive and in 1 M AQDS only 27% of the molecules remained in monomeric form. [14] However, later studies showed that for AQDS, the main limitation for capacity utilization was not aggregation but rather the formation of AQDS-CO_2 adducts especially when cycled in carbonated supporting electrolytes. [52]

Reduced viologens (Vi•+) π-dimerize through radical-radical stacking. This reduces the effective concentration of active species in the solution and slows down the diffusion. Steric or charged substituents, host-guest encapsulation or the addition of molecular spectators can suppress this association and improves the stability and performance of viologens. [53–55]

In NDIs, their planar aromatic cores strongly favor π-π stacking and aggregation. Early electrochemical studies revealed that NDIs undergoes strong dimerization. Although the dimer retained limited redox activity in cyclic voltammetry and rotating disk electrode measurements, it was believed that its fast dissociation allowed near-theoretical capacities to be achieved in bulk electrolysis. [15] Another study demonstrated that π-π stacking is the main barrier to solubility and electrochemical utilization with methyl NDIs being nearly insoluble in water due to extensive aggregation. To counteract this, ammonium-functionalized NDIs introduced electrostatic repulsion that disrupts stacking and raises solubility to 0.7 M in water. [45–47] More advanced strategies include regional charge buffering through electron-donating core substituents which compresses the two redox steps into a single two-electron process while mitigating repulsive interactions and synergistic hydrogen-bond networks for example by imidazolium or hydroxyl functionalization that stabilize radical intermediates and balance aggregation forces. [43,50] Recent zwitterionic modifications further tune π-π stacking into parallel-staggered structure, suppressing side-chain decomposition and achieving solubility up to 1.5 M in water. [49] In conclusion, the high capacity utilization observed in most of the NDI-based flow batteries suggests that self-association does not significantly hinder the performance. In some cases, self-association of reduced NDI species has even been shown to protect radical anions from undergoing side reactions, although it can also reduce solubility and alter the electrochemical behavior of NDIs. [47]

2.5 Flow Battery Performance Parameters

The performance of flow batteries is governed by several parameters as listed below:

- Theoretical volumetric capacity ($Q_{\text{theoretical}}$): The theoretical volumetric capacity of a battery is typically expressed in ampere-hours per liter (Ah/L) and shows the maximum amount of the charge that ideally the flow battery can deliver and depends on the number of electrons transferred per molecule (n), Faraday's constant (F), and concentration of redox-active molecules (c) and is expressed as:

$$Q_{\text{theoretical}} = nFc \tag{1}$$

- Energy density (E): The energy density in flow batteries describes the average energy stored per volume and is typically expressed in Watt-hours per liter (Wh/L) and depends on the volume of the electrolytes (V_{pos} and V_{neg}) and the cell potential (ΔV).

$$E = \frac{Q_{theoretical,pos} \times V_{pos} \times \Delta V}{(V_{pos} + V_{neg})} = \frac{Q_{theoretical,neg} \times V_{neg} \times \Delta V}{(V_{pos} + V_{neg})} \tag{2}$$

- Coulombic efficiency (CE): CE is a ratio of discharge to charge capacity and it is a good indication of electron loss that can happen due to side reactions or crossover.

$$\text{CE (\%)} = \frac{Q_{\text{discharge}}}{Q_{\text{charge}}} \times 100 \tag{3}$$

- Voltage efficiency (VE): VE is the ratio of average voltage during discharge to the average voltage during charge and is an indication of the overpotentials in the flow battery.

$$\text{VE (\%)} = \frac{V_{\text{discharge}}}{V_{\text{charge}}} \times 100 \tag{4}$$

- Energy efficiency (EE): EE is a ratio of the average energy accessed during the discharge process to the average energy spent during the charge process and is the product of CE and VE.

$$\mathrm{EE}\ (\%) = \frac{E_{\mathrm{discharge}}}{E_{\mathrm{charge}}} \times 100 = \mathrm{CE} \times \mathrm{VE} \tag{5}$$

- Capacity utilization (CU): CU refers to the fraction of the theoretical capacity accessed during the discharge process.

$$\mathrm{CU}\ (\%) = \frac{Q_{\mathrm{discharge}}}{Q_{\mathrm{theoretical}}} \times 100 \tag{6}$$

- Capacity loss: Capacity loss refers to the gradual loss in accessible discharge capacity and serves as an indication of the long-term performance and chemical stability of the redox-active molecules in the flow battery.

$$\text{Capacity Loss per cycle}\ (\%) = \frac{\Delta Q_{\mathrm{discharge}}}{(\text{total number of cycles}) \times intial\ capacity} \times 100 \tag{7}$$

$$\text{Capacity Loss per day}\ (\%) = \frac{\Delta Q_{\mathrm{discharge}}}{(\text{total cycling time}) \times intial\ capacity} \times 100 \tag{8}$$

State of charge (SOC): SOC refers to the current charge level of the flow battery relative to its maximum capacity and is directly linked to the concentration of the redox-active molecules in their oxidized or reduced forms at any time. [56–58]

$$\text{SOC of the positive side}(\%) = \frac{[\mathrm{Ox}]}{[\mathrm{Ox}]+[\mathrm{Red}]} \times 100 \tag{9}$$

$$\text{SOC of the negative side}(\%) = \frac{[\mathrm{Red}]}{[\mathrm{Ox}]+[\mathrm{Red}]} \times 100 \tag{10}$$

3 Materials and Methods

3.1 Materials

All purchased chemicals used in the publications that support this thesis were used as received without further purification.

In **Publication I**, 1,4,5,8-naphthalenetetracarboxylic acid dianhydride was purchased from TCI Chemicals, while gamma-aminobutyric acid and DMSO were supplied by Sigma-Aldrich and VWR, respectively.

In **Publication II**, 1,4,5,8-naphthalenetetracarboxylic acid dianhydride was purchased from TCI Chemicals. Potassium hydroxide, sodium hydroxide, aspartic acid, and hydrochloric acid were from Sigma-Aldrich, and DMSO was supplied by VWR.

In **Publication III**, 9,10-anthraquinone-2,7-disulfonic acid (98%, AQDS) was purchased from BossChemicals. Urea, phosphoric acid (85%), and trisodium phosphate (96%) were from Sigma-Aldrich. Naphthalene diimide derivatives (quaternary amine-functionalized NDI (D-NDI) and gamma-aminobutyric acid-functionalized NDI (GABA-NDI)) were synthesized according to previously reported procedure in the literature and as described in **Publication I.** [15,19]

3.2 Characterization Methods

Several analytical and electrochemical techniques were used to investigate the chemical and electrochemical properties of the studied molecules.

3.2.1 Cyclic Voltammetry

Cyclic voltammetry measurements (CV) were employed across all of the publications to evaluate the redox behavior of the studied RAOMs such as redox potentials and reversibility of the redox reactions.

CV experiments were performed using a standard three-electrode setup. A 3 mm in diameter glassy carbon working electrode from BASI was polished with 0.05 µm alumina slurry from Buehler and sonicated for one minute prior to each measurement. An Ag/AgCl electrode either 3 M KCl from Redox.me with potential of 212 mV vs. standard hydrogen electrode (SHE) (**Publication I** and **III**) or saturated KCl with potential of 197 mV vs. SHE (**Publication II**) along with a platinum wire as the counter electrode were used to complete the setup. Voltammograms were recorded at different scan rates of 20, 50, 100, 250, and 500 mV/s (only in **Publication I**) with 90% *iR*-correction. All measurements were conducted in triplicate to ensure reproducibility of the voltammograms. The electrochemical data were recorded with Gamry Reference 620 (**Publication I and III**) or Biologic SP-300 potentiostat (**Publication II**).

3.2.2 Rotating Disk Electrode

Rotating disk electrode measurements (RDE) were used to investigate the diffusion-controlled electrochemical behavior of the studied redox-active molecules in all publications.

RDE experiments were performed using a 5 mm in diameter glassy carbon working electrode from Metrohm that was polished with 0.05 µm alumina from Buehler and sonicated for one minute prior to each measurement. An Ag/AgCl electrode either 3 M KCl from Redox.me with potential of 212 mV vs. SHE (**Publication I** and **III**) or saturated KCl with potential of 197 mV vs. SHE (**Publication II**) along with a platinum wire as the counter electrode were used in the three-electrode setup. The RDE setup consisted of an Autolab RDE motor and Gamry Reference 620 for **Publication I** and **III**, and Pine Instruments MSR RDE analytical rotator and a CH Instruments bipotentiostat (CHI760E) for **Publication II**. Voltammograms were recorded at a scan rate of 5 mV/s, at rotation rates of 400, 900, 1600, 2500, and 3600 rpm with 90% *iR*-correction. All measurements were done in triplicate to ensure reproducibility.

3.2.3 Electrochemical Impedance Spectroscopy

Electrochemical impedance spectroscopy (EIS) at the open circuit potential (OCP) was done to determine the ohmic resistance of the assembled flow batteries and solution resistance (R_s) values were extracted from the high-frequency intercept of the Nyquist plot with the real axis as shown in Figure 6. Prior to cycling flow batteries in **Publication I-III**, the batteries was circulated with electrolyte for one hour and then EIS was done with a Biologic SP-240 potentiostat. In **Publication I**, the cut-off voltages used were corrected according to the ohmic losses (*iR*) at each current density.

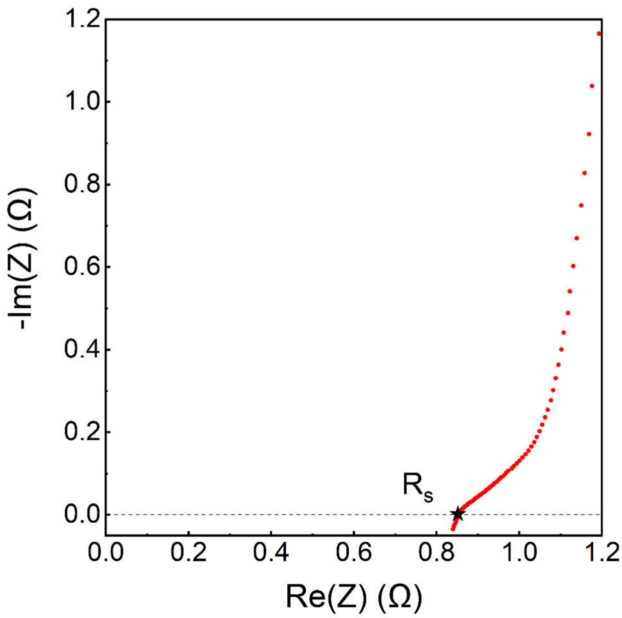

Figure 6. EIS on a 500 mM ASP-NDI/ sodium ferrocyanide ($Na_4[Fe(CN)_6]$) with Fumasep E-630 (K).

3.2.4 Flow Battery Measurements

The cycling stability of the synthesized NDI molecules were evaluated using custom-built lab-scale flow battery cells. Carbon felts with the active area of 5 cm² and the thickness of 4.6 mm were used as electrodes and compressed to approximately 3 mm after cell assembly. Membranes were pre-soaked in the corresponding supporting electrolyte for 2 hours (**Publication II** and **III**) and 1 day (**Publication I**) prior to use. Compressible expanded PTFE gaskets were used to provide sealing in the cell. Chonry BT600M peristaltic pump with Masterflex C-Flex tubing from Cole-Parmer was calibrated to deliver a desired flow rates throughout the experiments. Battery cycling measurements were done using LANHE (**Publication I** and **III**) and Neware BTS-400 cyclers (**Publication II**). The electrolytes were made with deionized water and the excess amount of electrolyte in the positive side always assured that the negative side is limiting in all of the studied flow batteries. The cut-off voltages for charge and discharge are stated in the publications. Two of the studied flow batteries in **Publication I** and **Publication III** were operated inside a nitrogen-filled MBraun glovebox and one flow battery was operated in atmospheric air. In **Publication II** all of the flow batteries were cycled in sealed boxes constantly purged with nitrogen throughout the cycling with O_2 levels of around 200 ppm. Different cycling protocols were used to study the performance of NDI-based flow batteries as stated in the original publications. For stability assessment, extended galvanostatic cycling or constant current (CC) at 60 mA cm^{-2} (**Publication I** and **III**) and 20 mA cm^{-2} (**Publication II**) were applied.

3.2.5 Nuclear Magnetic Resonance

Nuclear magnetic resonance spectroscopy (NMR) was used throughout this research for multiple purposes. Initially, NMR was employed to confirm the molecular structure of the synthesized molecules. Additionally, it was used to evaluate the solubility of these molecules in deionized water. After flow battery cycling, NMR was utilized to detect possible chemical degradation or side products. In **Publication III**, NMR helped us to study the self-association behavior of RAOMs.

NMR measurements in **Publication I** and **III** were done with Bruker 500 MHz spectrometer and in **Publication II** with bench-top 80 MHz Magritek Spinsolve spectrometer.

3.2.6 Elemental Analysis and Inductively Coupled Plasma Mass Spectrometry

To verify the composition and degree of ion exchange in ammonium ferrocyanide that was used in **Publication I**, elemental analysis (CHN) and inductively coupled plasma (ICP) spectroscopy were employed. CHN analysis was performed to determine the carbon, hydrogen, and nitrogen content of the synthesized samples. ICP-OES was used to determine the amounts of sodium and iron in the samples to support CHN analysis. Moreover, CHN analysis was done on GABA-NDI to confirm its structure.

3.2.7 Liquid Chromatography-Mass Spectrometry

Liquid chromatography-mass spectrometry (LC-MS) was employed to characterize the structure and purity of the synthesized NDI in **Publication II**. Chromatographic separation was performed using a C18 reverse-phase column. Electrospray ionization (ESI) in positive mode was used for mass detection.

4 Results and Discussions

This chapter presents the design, synthesis, and electrochemical evaluation of two new water-soluble naphthalene diimides (NDIs) namely GABA-NDI and ASP-NDI and investigates their performance in flow battery. Structural confirmation and solubility were studied by ^{1}H-NMR followed by electrochemical characterization. Cyclic voltammetry revealed two reversible one-electron reductions for both NDIs with negligible scan-rate dependency. Rotating-disk electrode measurements provided diffusion coefficients on the order of 10^{-6} cm^2 s^{-1} and confirmed concentration-dependent self-association. Flow-battery experiments demonstrated fast kinetics across a wide current density range but also showed that exposure to air led to SOC imbalance. The long-term cycling stability of NDI-based flow batteries in our study depends on membrane selectivity and water transport. Insufficient selectivity can lead to crossover of active species, while water transport causes volume imbalance and concentration drift and both of these contribute to the capacity fade during extended cycling. Post-mortem NMR analysis confirmed no detectable decomposition of both studied NDIs. Finally, the self-association behaviour of NDIs and AQDS was investigated in the presence of urea. Although NMR and electrochemical data indicated partial disruption of aggregation, the flow battery performance did not improve much.

4.1 Synthesis of Naphthalene Diimides

In this thesis, two novel water-soluble NDI derivatives were synthesized: one functionalized with γ-aminobutyric acid (GABA) and the other with aspartic acid (ASP) to evaluate how functional group modification affects aqueous solubility, redox potential and flow battery performance of the water-soluble NDIs. Functionalization of the NDIs with GABA or ASP both occurred in a one-step synthesis as discussed in **Publication I** and **II** and the synthesized molecules will be simply referred to as GABA-NDI and ASP-NDI in this thesis. The protonated structures of these molecules are shown in Figure 7.

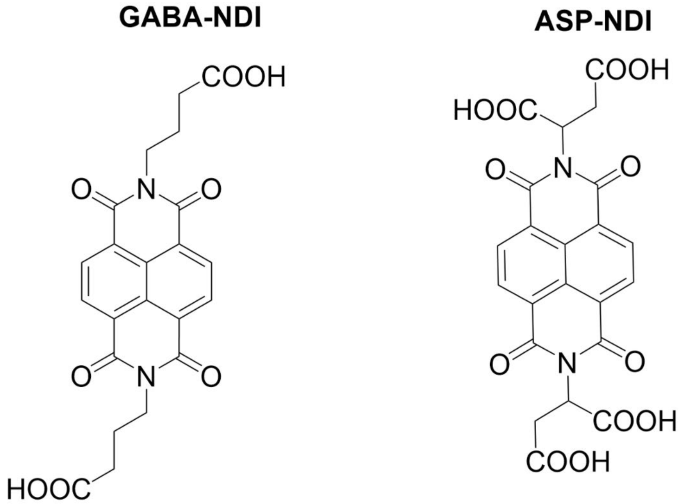

Figure 7. GABA-NDI and ASP-NDI in their protonated form.

4.1.1 Structural Characterization

The successful synthesis of NDIs was confirmed with ^{1}H-NMR and no sign of any impurity was seen in the spectra. Characteristic aromatic and aliphatic proton signals in both of the molecules were consistent with the expected structure as shown in Figure 8 and Figure 9. In addition, ^{1}H-NMR was also used to determine solubility of the molecules by relating the signal intensity to that of the internal reference with known concentration as explained in more details in the supporting information of the publications. With this method, the solubility of GABA-NDI is measured to be 0.587 M and ASP-NDI is 1.07 M in DI water. The almost three-fold in water increase in the solubility of GABA-NDI compared to B-NDI arises from the longer alkyl linker between the NDI core and the terminal carboxyl group. GABA-NDI contains three methylene spacers, whereas B-NDI has only one. Extending the alkyl chain increases the spatial separation between adjacent NDI cores and therefore weakens the π–π stacking and reduces molecular aggregation. Similar effect was also observed in other modified NDIs. [49,50] The two-fold increase in the solubility of ASP-NDI in comparison to GABA-NDI in water is related to the presence of one additional carboxylic acid group on aspartic acid that increases the hydrophilicity of the molecule. [58,59]

In **Publication II**, LC-MS analysis was done to further confirm the structure of the ASP-NDI and as showed in the supporting information of the publication, the major peak corresponded to the expected molecular mass of the fully substituted ASP-NDI compound.

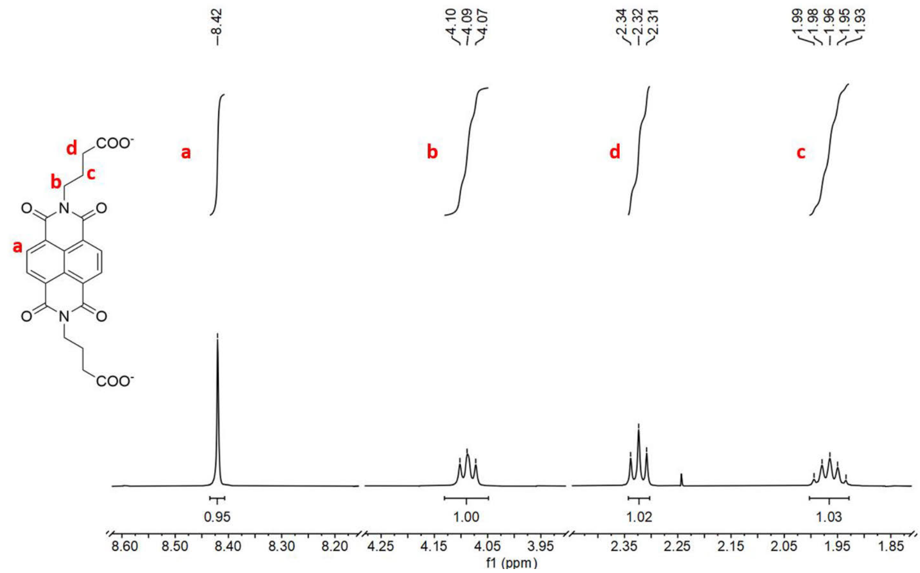

Figure 8. ^{1}H-NMR specta after the synthesis of GABA-NDI in DMSO.

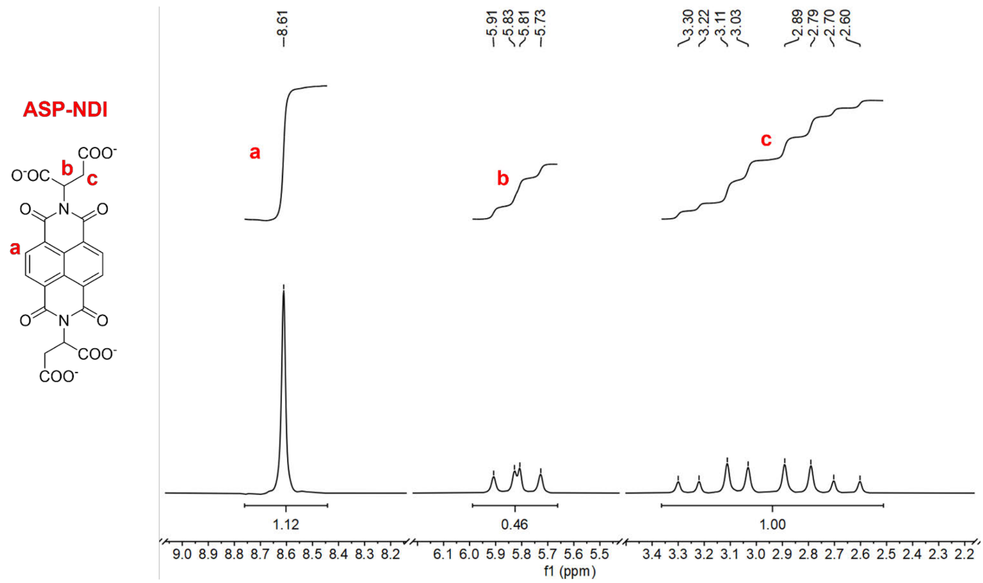

Figure 9. ^{1}H-NMR specta after the synthesis of ASP-NDI in 1 M NH_4Cl.

4.1.2 Effect of Functionalization on Ionic Environment

We quantified the ionic environments in the GABA-NDI and ASP-NDI half-cells before and after cycling using the classical expression for ionic strength:

$$\text{Ionic Strength (I)} = \frac{1}{2}\sum c_i z_i^2 \qquad (10)$$

The calculated values are summarized in Table 2. For a 100 mM GABA-NDI electrolyte in 1 M NH_4Cl, the ionic strength increased from 1300 mM before cycling to 2000 mM after cycling with the average of 1650 mM. Under identical conditions, the ASP-NDI electrolyte exhibited higher values, rising from 2000 mM to 3100 mM with the average of 2550 mM. The corresponding ferri/ferrocyanide electrolyte decreased from 2000 mM to 1600 mM with the average of 1800 mM. These results show that, at equal active-species concentration, ASP-NDI generates a significantly higher ionic-strength environment than GABA-NDI. This can influence the Donnan exclusion and crossover behaviour across the cation-exchange membrane. [60]

Table 2. Ionic strength and osmolarity before and after cycling for ASP-NDI and GABA-NDI flow batteries.

SPECIES	CONDITION	CHARGE	CONCENTRATION	I (mM)
GABA-NDI	before cycling	-2	100 mM	1300
	after cycling	-4	100 mM	2000
ASP-NDI	before cycling	-4	100 mM	2000
	after cycling	-6	100 mM	3100
Ferri/Ferro cyanide	before cycling	-4	100 mM	2000
	after cycling	-3	100 mM	1600

4.2 Electrochemical Characterization of NDIs

4.2.1 Cyclic Voltammetry of NDIs

The CV experiments at various scan rates revealed two reversible one-electron redox processes for both synthesized NDI derivatives first to the radical anion and then to the dianion. The average redox potential for GABA-NDI and ASP-NDI is −459mV and −551 mV, respectively as shown in Figure 10 that raises the total cell voltage by 65.5 mV. The observed decrease in redox potential from GABA-NDI to ASP-NDI is attributed to the presence of an additional carboxylate group in the aspartic acid moiety which increases the electron-donating character of the substituent. [61] The redox potentials of both GABA-NDI and ASP-NDI remained almost unchanged with increasing scan rate that indicates fast electron-transfer kinetics. However, as shown in **Publication I** and **II**, the concentration-normalized CVs did not overlap and the peak currents decreased with increasing concentration as shown in Figure 11 for ASP-NDI. This behaviour indicates a tendency for self-association of NDI molecules at higher concentrations due to the π-π interactions. Additionally, adsorption of species on the electrode could affect this response.

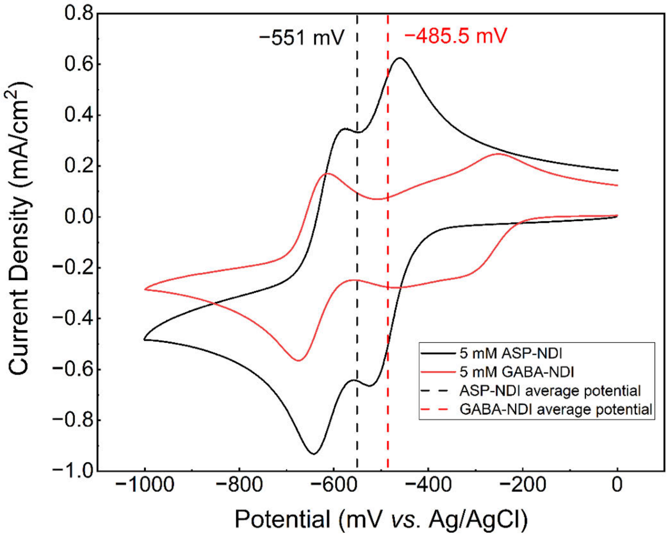

Figure 10. CV at 100 mV/s on the GABA-NDI and ASP-NDI in 1 M NH_4Cl.

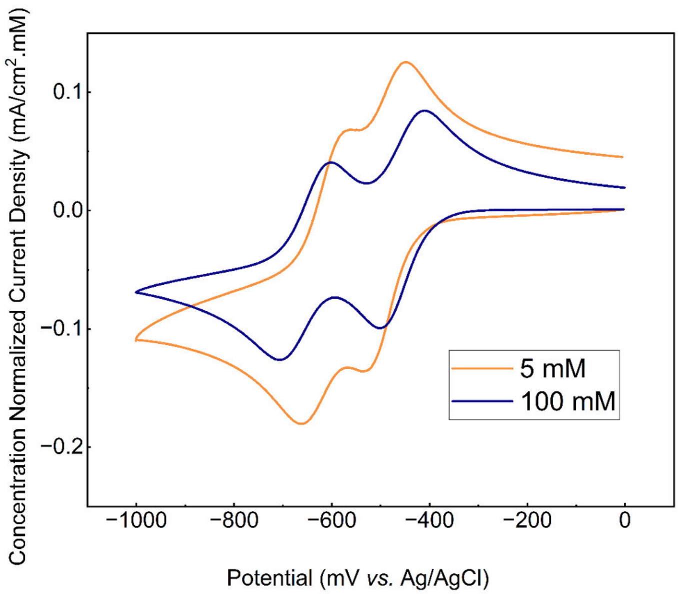

Figure 11. Concentration dependency of the CV of ASP-NDI.

The electrochemical behaviour of ASP-NDI was investigated in different pH values starting from pH 7. As shown in Figure 12, the redox processes remain stable up to pH 10.5 indicating consistent activity of the molecule within this pH window. Based on these measurements and as shown in **Publication II**, the first reduction exhibits slope of –0.9 mV/pH between pH 7-8.5 and –12 mV/pH between pH 8.5-10.5 while the second reduction shows a slope of –1.1 mV/pH over pH 7-10.5. These small changes suggest that the redox reactions are insensitive to pH variation in this range. This is in agreement with previous reports on quaternary amine-functionalized NDIs. [15] However, prolonged exposure of ASP-NDI to pH 10.5 leads to hydrolysis of the imide rings that results in ring opening and subsequent loss of electrochemical activity. [62]

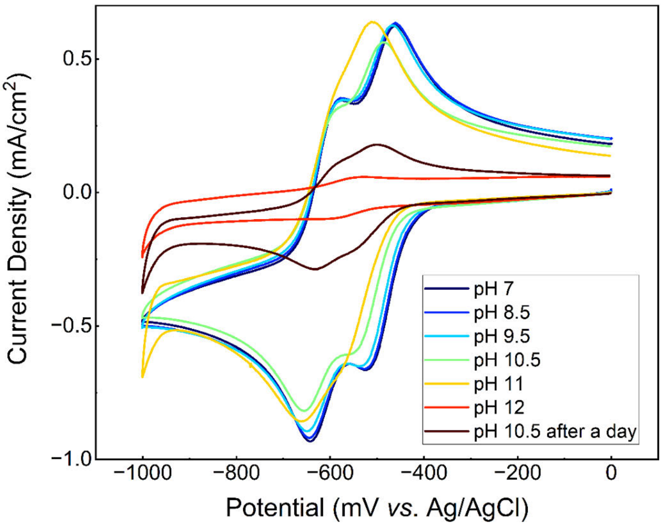

Figure 12. pH dependency of 5 mM ASP-NDI in 1 M NH_4Cl and 0.5 M ammonium phosphate buffer at 50 mV/s.

4.2.2 Rotating disk electrode measurements on NDIs

To further evaluate the diffusion behaviour and estimate the diffusion coefficients of the NDIs, RDE was performed at different rotation rates. RDE of GABA-NDI is shown in Figure 13 as an example. As expected, the limiting currents increased with the square root of the rotation rates. Diffusion coefficients for the both of the NDI derivatives were calculated from the Levich equation as discussed in the supporting information of the publications. Both molecules showed diffusion coefficients in the range of ~10^{-6} cm^2/s for the mixture of monomer and dimer which is typical for RAOMs in aqueous electrolytes. [63] The self-association behaviour of the molecules is also evident in the RDE results. Specifically, the first reduction current is larger than the second although both processes correspond to a one-electron reduction. This discrepancy is related to the self-association of NDIs.

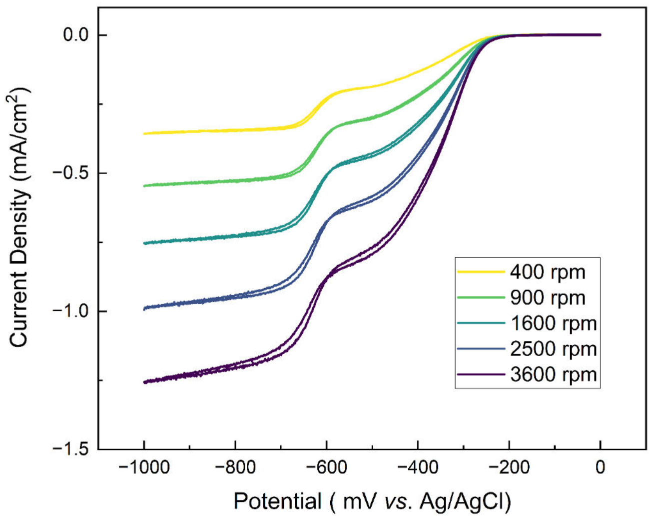

Figure 13. RDE on 1 mM GABA-NDI in 1 M NH_4Cl at different rotation rates.

4.2.3 Flow Battery Measurements on GABA-NDI

The flow battery experiments in **Publication I** were performed using 200 mM of GABA-NDI as the negative electrolyte and 200 mM of ammonium ferrocyanide ($(NH4)_4[Fe(CN)_6]$) as the positive electrolyte with an average voltage of 0.76 V across Selemion SX-053DK. Three flow batteries at different conditions were studied: buffered flow battery, unbuffered flow battery, and air-exposed flow battery. The supporting electrolytes in the buffered flow battery was 1 M ammonium chloride (NH_4Cl) + 0.5 M ammonium phosphate and in the unbuffered one was 1 M NH_4Cl. These two batteries were cycled in a nitrogen-filled glovebox while in the air battery, the supporting electrolyte was 1 M NH_4Cl and the battery was cycled in the atmospheric air. Both of the flow batteries cycled in the glovebox exhibited high CU of around 95% with CE of 99.9% and EE of around 70% for the whole cycling duration as shown in Figure 14. In both cases, a gradual pH drop during long-term cycling and osmosis from the ferrocyanide side to the NDI side led to the precipitation of GABA-NDI on the carbon felt and in the tubing as shown in the supporting information of **Publication I** and resulted in capacity loss. The buffering strategy did not effectively stabilize the pH, since the NH_4^+/NH_3 equilibrium is disturbed by the evaporation of volatile ammonia during degassing. Although using buffered supporting electrolyte could not maintain the pH, buffered flow battery showed slightly improved stability in comparison to the unbuffered system. CV and

NMR analysis after both of these flow batteries confirmed no visible decomposition of GABA-NDI or crossover of any of the species through the Selemion SX-053DK membrane.

The air battery demonstrated significant performance degradation within the first few cycles due to oxidation of the reduced GABA-NDI with the atmospheric oxygen that results in SOC imbalance and capacity fade. Even after replacing the positive electrolyte and moving the battery into a glovebox, the capacity did not recover and further cycling confirmed irreversible capacity loss likely due to slight decomposition of NDIs.

In summary, **Publication I** presents a newly developed NDI molecule that carries negative charges in aqueous solution and emphasizes the critical role of maintaining an inert atmosphere and stable pH during the cycling of the GABA-NDI based flow batteries, while also identifying water crossover as a key limitation for long-term operation of the AOFBs.

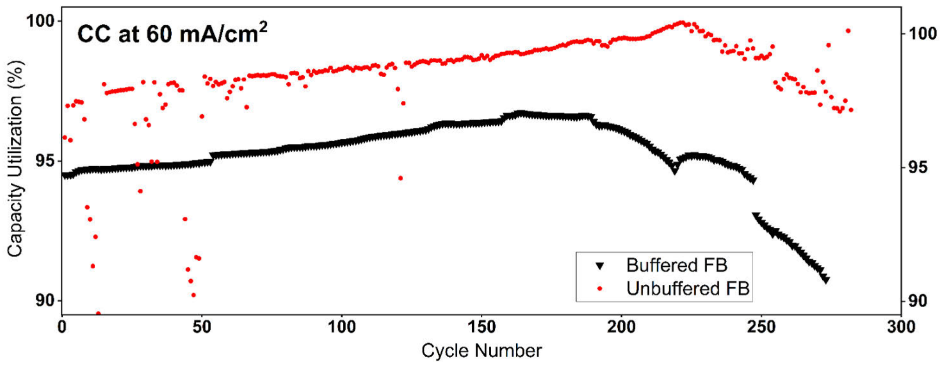

Figure 14. Flow battery performance of 200 mM GABA-NDI/ $Na_4[Fe(CN)_6]$ at 60 mA/cm^2.

4.2.4 Flow Battery Measurements on ASP-NDI

To evaluate the performance of ASP-NDI in flow battery in **Publication II**, four flow batteries were assembled using the same redox couples of ASP-NDI in the negative electrolyte and $Na_4[Fe(CN)_6]$ in the positive electrolyte but varying in concentration and membrane type labelled as FB 1 to 4 as shown in Table 3. The average cell voltage is approximately 0.82 V which is 53 mV higher than in GABA-NDI flow batteries. Cycling experiments over a wide current density range from 5 to 60 mA cm^{-2}, demonstrated fast kinetics consistent with earlier results obtained for GABA-NDI in **Publication I** as shown in Figure 15. [19]

Table 3. Flow batteries made with ASP-NDI in **Publication II**.

	FB 1	**FB 2**	**FB 3**	**FB 4**
Negative electrolyte	100 mM ASP-NDI	500 mM ASP-NDI	100 mM ASP-NDI	500 mM ASP-NDI
Positive electrolyte	100 mM $Na_4[Fe(CN)_6]$	500 mM $Na_4[Fe(CN)_6]$	100 mM $Na_4[Fe(CN)_6]$	500 mM $Na_4[Fe(CN)_6]$
Membrane	Selemion SX-053DK	Selemion SX-053DK	Fumasep E630 (K)	Fumasep E630 (K)
Cycling time at 20 ma/cm^2	11.51 days	9.83 days	13.86 days	79.84 days
Capacity loss for the long cycling at 20 ma/cm^2	0.017 % per cycle 0.382 % per day 139.25 % per year average CE (%): 99.95	0.036 % per cycle 0.175 % per day 63.75 % per year average CE (%): 99.87	0.011 % per cycle 0.260 % per day 94.77 % per year average CE (%): 99.97	0.010 % per cycle 0.0275 % per day 10.04 % per year average CE (%): 99.93
Temperature in the box (◦c)	in the beginning: 26.5 at the end: 29.5	in the beginning: 27 at the end: 31	in the beginning: 26.7 at the end: 29.5	in the beginning: 25 at the end: 32

Table 4. Membranes used in **Publication II** and their characteristics.

MEMBRANE	**COUNTER-ION**	**THICKNESS (µm)**	**IEC (mmol/g)**
FUMASEP E630 (K) [64]	K^+	34	1.1
SELEMION SX-053DK [65]	K^+	50	-

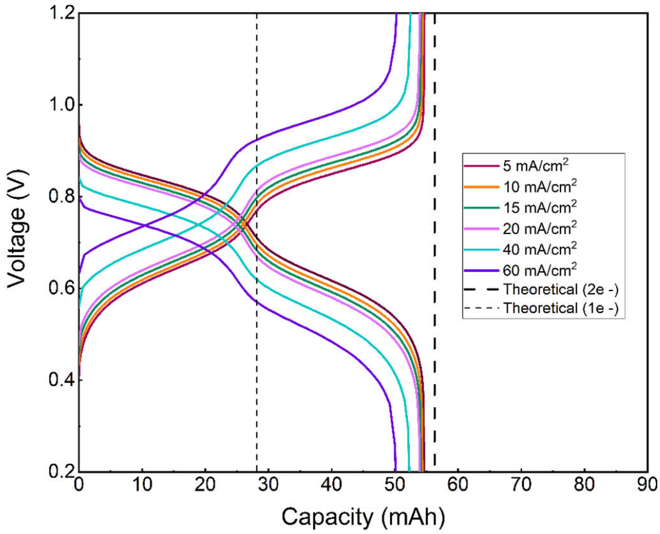

Figure 15. Representative charge/discharge curves of flow battery consisting of 10.5 mL of 100 mM ASP-NDI vs 33 mL of 100 mM of $Na_4[Fe(CN)_6]$ in 1 M NH4Cl and 0.5 M ammonium phosphate buffer at pH 7.9.

FB 1 and FB 3 were both operated with 100 mM ASP-NDI/100 mM $Na_4[Fe(CN)_6]$ electrolytes under similar conditions but employed different CEMs: Selemion SX-053DK in FB 1 (Figure 16) and Fumasep E-630(K) in FB 3 (Figure 17). Despite both being CEMs, the Fumasep membrane showed slightly better stability with a lower per-cycle capacity fade (0.011% per cycle, 0.260% per day) compared to Selemion (0.017% per cycle, 0.382% per day) while exhibiting nearly similar EE and CE values. Post-mortem CV analysis revealed that in FB 1, Selemion permitted some crossover of ferrocyanide ions ($[Fe\ (CN)_6]^{4-}$) into the ASP-NDI side. By contrast, no such crossover was detected after FB 3 (Figure 18). Although according to Table 4 Selemion SX-053DK is thicker than Fumasep E-630(K), it exhibited both lower resistance crossover as shown in Figure 19 and higher crossover. This can be explained by its higher water uptake that lowers the resistance and enhances the diffusion.[65] Moreover, although FB 3 exhibited slightly slower capacity fading, this relatively small difference can indicate that membrane selectivity alone cannot fully explain the observed decay. There are other factors that contribute to the capacity loss that are common to both systems. These factors are osmotic water transport, electro-osmotic drag and slow evaporation from the reservoirs due to the continuous heat generation by the peristaltic pumps can cause gradual electrolyte imbalance and apparent capacity loss even when there is no crossover. These operational effects are consistent with the high and stable coulombic efficiencies (≈99.9%) observed for both flow batteries and suggest that the primary capacity fade arises from physical processes rather than parasitic reactions or chemical decomposition (as further confirmed by NMR analysis). The improved performance of Fumasep is likely due to its greater ionic selectivity and reduced permeability over prolonged cycling. Moreover, long-term flow battery operation can compromise the anion-blocking ability and selectivity of Selemion membranes, most likely because of electro-osmotic drag and water transport across the membrane. This observation aligns with **Publication I** in which the same Selemion SX-053DK membrane showed no detectable crossover under shorter cycling durations. [66,67]

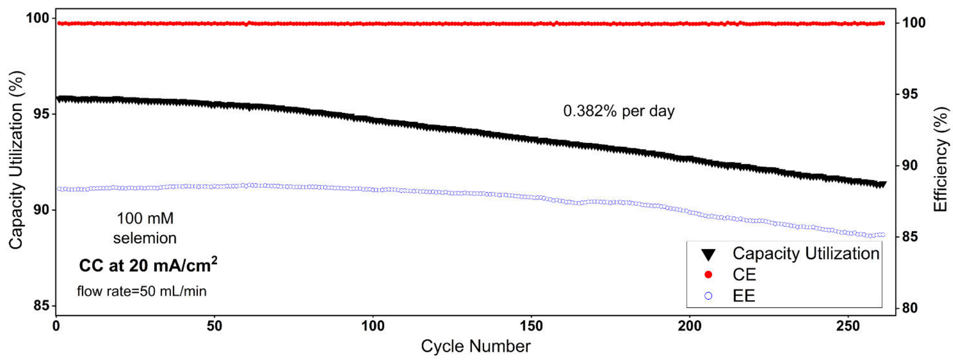

Figure 16. Long term performance of FB 1 with 100 mM ASP-NDI vs 100 mM $Na_4[Fe(CN)_6]$ with Selemion SX-053DK membrane at 20 mA/cm^2 with total cycling time of 11.6 days.

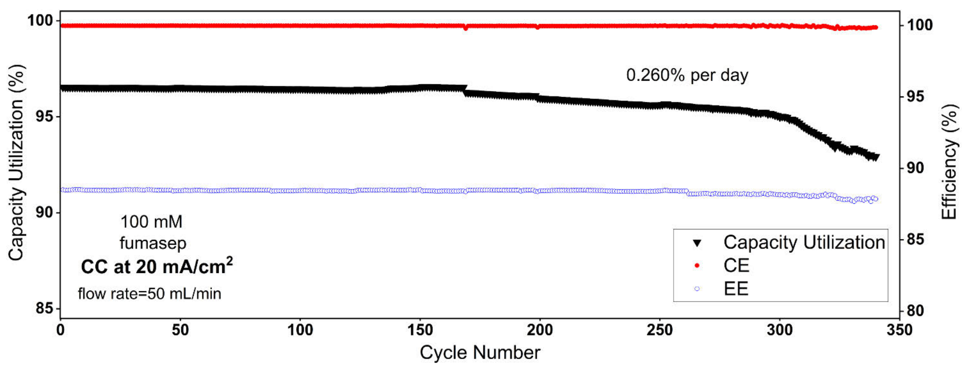

Figure 17. Long term performance of FB 3 with 100 mM ASP-NDI vs 100 mM $Na_4[Fe(CN)_6]$ with Fumasep 630 (K) membrane at 20 mA/cm^2 with total cycling time of 14 days.

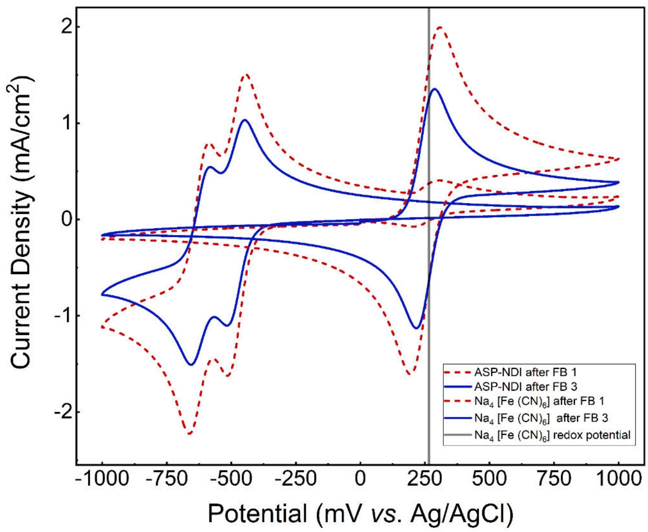

Figure 18. CV after FB 1 and FB 3 on ASP-NDI and Na_4 [Fe (CN)$_6$].

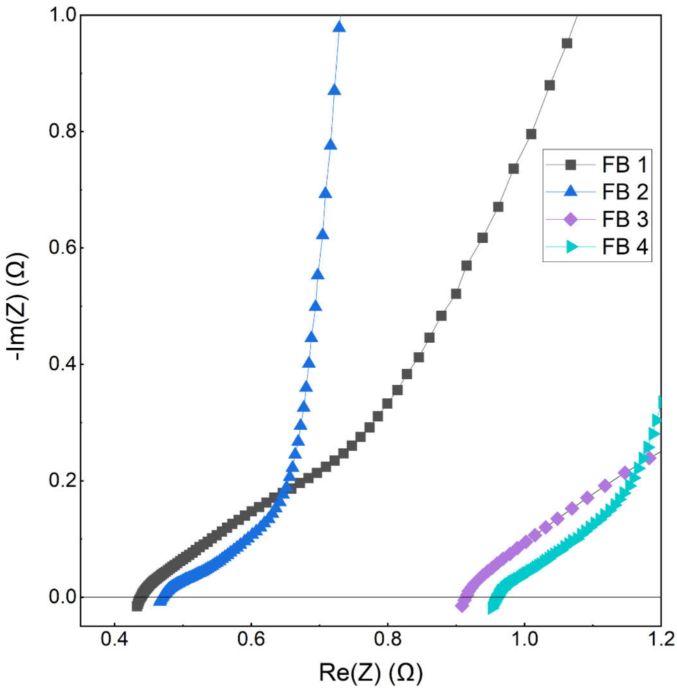

Figure 19. Nyquist plots for EIS of the studied flow batteries in this work before cycling.

At higher concentration of 500 mM ASP-NDI/500 mM $Na_4[Fe(CN)_6]$, the performance difference between the two CEMs became more evident. FB 2 with Selemion SX-053DK in Figure 20 showed a capacity fade of 0.036% per cycle (0.175% per day), while FB 4 operating with Fumasep E-630(K) in Figure 21 exhibited a lower fade of 0.015% per cycle (0.28% per day) and operated stably for nearly 80 days compared to only 10 days for FB 2. These FBs delivered high CE of around 99.8% and good EE of 90.6% for FB 2 and 87.5% for FB 4. However as shown in Figure 22, FB 2 suffered from $[Fe (CN)_6]^{4-}$ crossover while Fumasep provided stable stability over hundreds of cycles. In this study the capacity fade of the higher-concentration batteries was lower than that of the lower-concentration ones, a trend also observed by X. Zhang *et al.* in their imidazolium-functionalized naphthalene diimide flow batteries.[50] Although Zhang et al. did not discuss the underlying cause of this behaviour, our results suggest that the capacity fade in our battery is not chemically driven; therefore, the fade rate remains independent of active-species concentration, since a chemically induced decay would typically scale with concentration. In addition, higher electrolyte concentrations increase the overall ionic strength, which lowers the diffusion coefficients of the species and can further suppresses crossover through the membrane.

To conclude, Selemion-based flow batteries (FB 1 and FB 2) consistently showed capacity decay due to ferrocyanide crossover. Whereas the Fumasep-based flow batteries (FB 3 and FB 4) achieved significantly longer lifetimes with stable cycling for 24.7 and 79.8 days respectively, compared to 13.6 and 17.5 days for the Selemion-based ones. Importantly, ^1H NMR analysis of the electrolytes after cycling confirmed no detectable chemical degradation of ASP-NDI in either of the flow batteries as shown in Figure 23 indicating that capacity fade in flow batteries with Selemion membrane is not due the molecular instability. It is worth mentioning again that water transfer from the negative to the positive side of the flow battery gradually concentrated the ASP-NDI electrolyte which over time promoted local precipitation particularly near electrodes or tubing junctions and contributed to capacity fade and flow resistance that is reflected by declines in energy efficiency in all of the tested flow batteries.

Additionally, the consistently high utilization of ASP-NDI in all flow batteries as others have also discussed can indicate that either the self-association in this molecule is reversible and the aggregates dissociate back to monomers during cycling or that aggregates are electrochemically active and therefore enable full access to the two-electron redox process. [15,47] This is in contrast with AQDS-based flow batteries where dimerization limits the achievable capacity especially in the presence of CO_2. [52]

To summarize this section, the best flow battery performance was achieved with ASP-NDI at a concentration of 500 mM using the Fumasep E-630(K) membrane in

FB 4. This system exhibited stable cycling for nearly 80 days with a capacity fade of only 0.0275% per day representing the lowest fade rate reported in the literature for NDI-based flow batteries. This highlights ASP-NDI as a highly promising candidate for long-term stable operation in AOFBs.

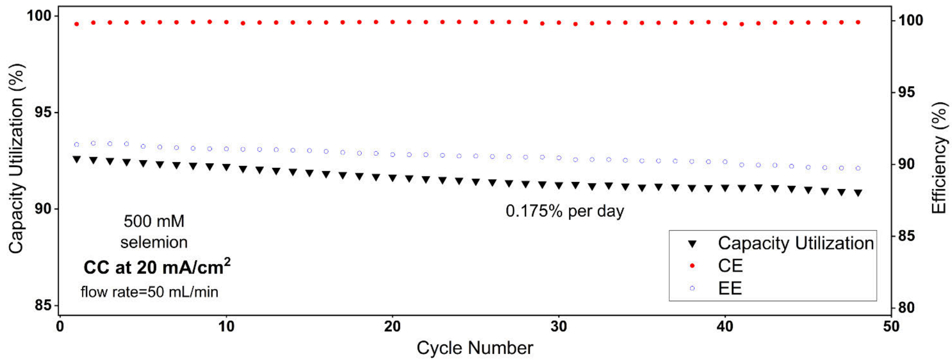

Figure 20. Long term performance of FB 2 with 500 mM ASP-NDI vs 500 mM Na_4 [Fe $(CN)_6$] with Selemion SX-053DK membrane at 20 mA/cm^2 with total cycling time of 10 days.

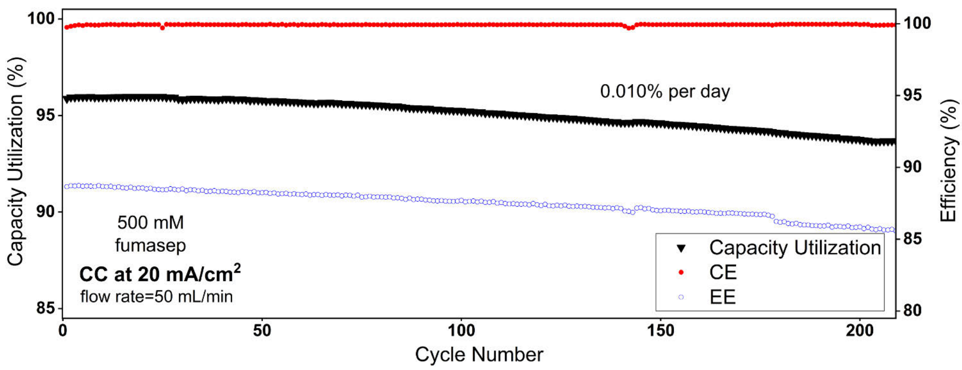

Figure 21. Long term performance of FB 3 with 500 mM ASP-NDI vs 500 mM Na_4 [Fe $(CN)_6$] with Fumasep 630 (K) membrane at 20 mA/cm^2 with total cycling time of 79.8 days.

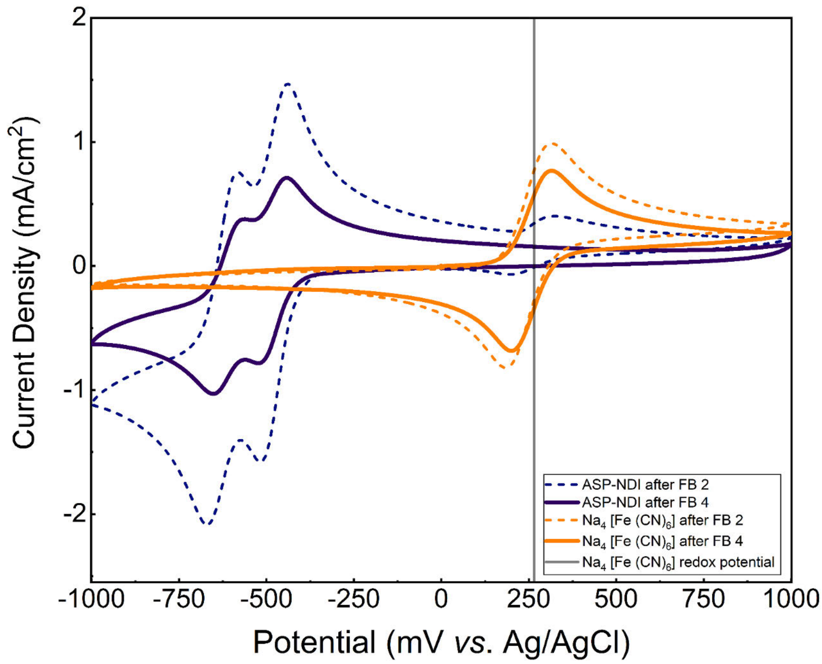

Figure 22. CV after FB 2 and FB 4 on ASP-NDI and Na_4 [Fe (CN)$_6$].

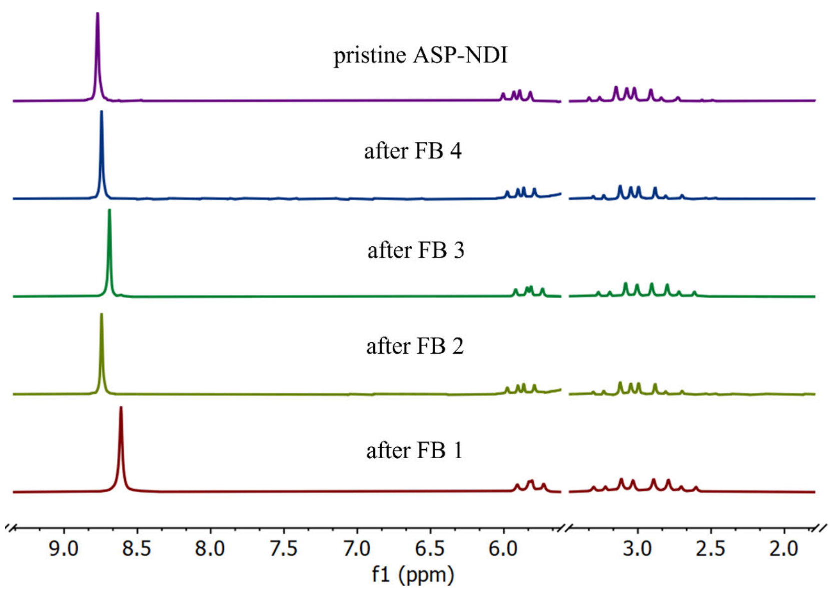

Figure 23. ^{1}H NMR after long-term flow battery cycling of ASP-NDI.

4.2.5 Self-association Study on AQDS and NDIs with NMR

As mentioned in chapter 2, self-association of RAOMs in aqueous solutions is one of the challenges in flow batteries as it limits their electrochemical performance. Both AQDS and NDI derivatives are prone to self-association through π-π stacking of their aromatic cores which could reduce the fraction of electrochemically active species, increases hydrodynamic radius and reduces diffusion coefficient. [14,15] **Publication III** investigates how the chaotropic additive urea can affect this behaviour using a combination of spectroscopic and electrochemical methods.

Urea is a small polar molecule capable of forming hydrogen bonds with water. By interacting with the hydrogen-bond network of water, it can increase the overall disorder of the solution and weaken hydrophobic interactions. At sufficiently high concentrations, these effects can shift the aggregation equilibrium of aromatic molecules toward their monomeric forms.[68] For example, urea has been shown to reduce the aggregation and increase the solubility of Azure B molecules in aqueous solution and to modify the solvation energy of ions. [69,70] Based on these properties, urea is expected to disrupt π-π stacking in RAOMs.

Building on the study of NDIs by Wiberg *et al.*, [15] NMR spectroscopy was employed to probe the molecular-scale environment of AQDS and NDIs. As shown in Figure 24 for AQDS and Figure 25 for GABA-NDI, increasing the concentration of both molecules led to upfield chemical shifts. In the case of GABA-NDI, additional signal broadening was observed in the aromatic region. Both observations are indicative of pronounced aggregation. Upon addition of urea, aromatic peaks shifted closer to those observed at dilute concentrations and peak broadening was reduced. These results demonstrate that urea can disrupt π-π interactions in the molecular level.

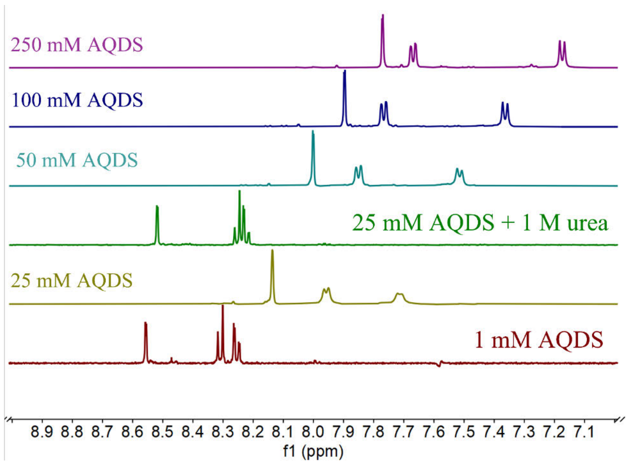

Figure 24. ^{1}H-NMR on concentration series of AQDS with and without urea in 1 M sodium carbonate buffer pH 9.5 in 10% D_2O.

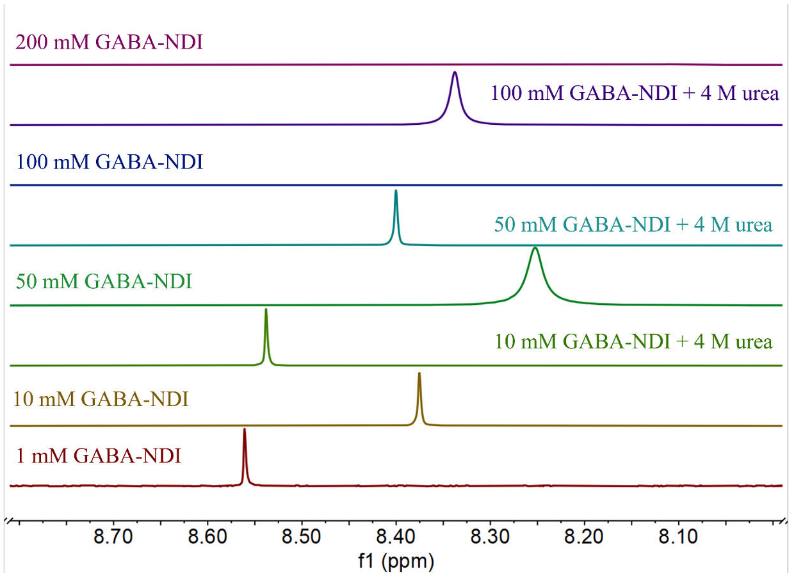

Figure 25. ^{1}H-NMR of the aromatic peak for a concentration series of GABA-NDI in 1 M NH4Cl in 10% D_2O with and without urea.

4.2.6 Self-association Study on AQDS and NDIs with Electrochemistry

To further investigate the impact of self-association on electrochemical behaviour, CV and RDE studies were employed. All CV and RDE data recorded in the presence of urea were normalized using a viscosity correction factor to account for the viscosity-dependent decrease in peak current as discussed in **Publication III**. CV of GABA-NDI revealed concentration-dependent shifts in redox potentials and increased peak separations which can indicate that π-π stacking hinders the electron-transfer kinetics. The addition of 4 M urea slightly reduced the peak separation and partially shifted the first reduction to more negative values suggesting partial disruption of aggregation as shown in Figure 26. However, the lack of overlap in concentration-normalized CVs confirmed that stacking was not fully suppressed in contrast to what was seen in the NMR spectra. CV of 25 mM AQDS in the presence of urea as shown in Figure 28a showed a gradual negative shift in both oxidation and reduction peaks. Figure 27 shows that redox potentials decreased linearly with increasing urea concentration. The current response, however, declined more than expected from viscosity effects alone. Comparison of the concentration-normalized CVs of 25 mM and 1 mM AQDS in Figure 28b revealed that urea showed a negative effect on the behaviour with smaller peak current than in the absence of urea. The peak currents for the concentrated solution with urea remained significantly lower than those of the dilute solution.

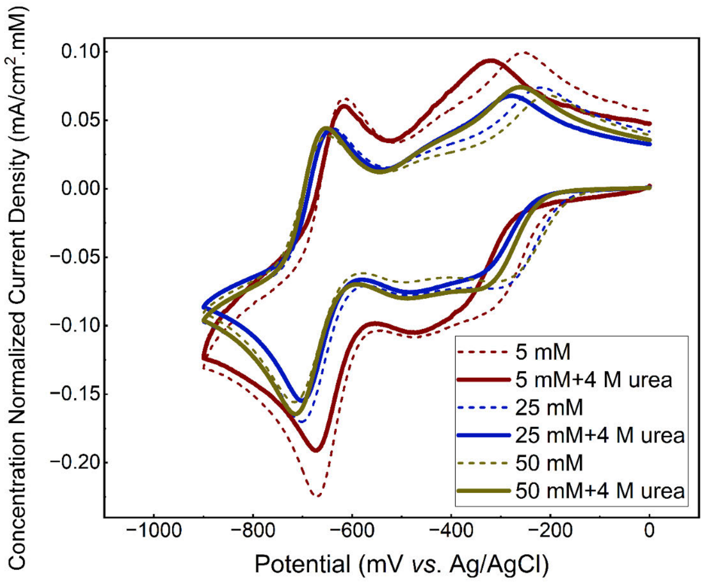

Figure 26. Concentration normalized CV of GABA-NDI at different concentrations without and with urea (viscosity corrected) in 1 M NH_4Cl at scan rate of 100 mV/s.

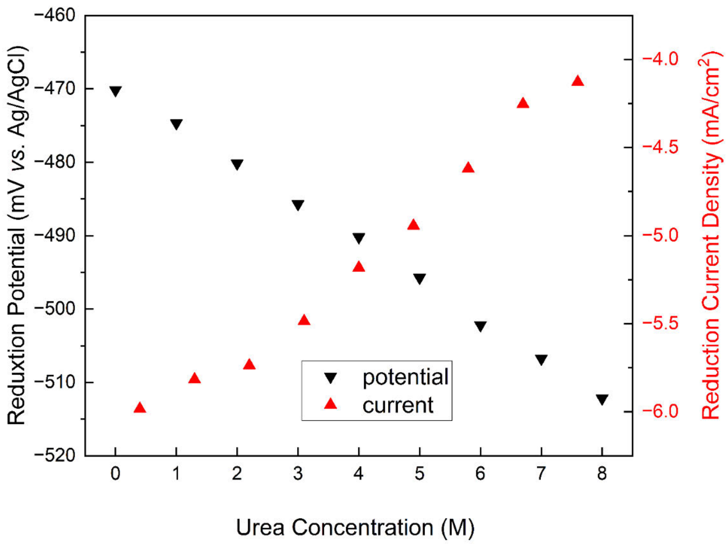

Figure 27. Reduction potential and reduction peak current density of 25 mM AQDS as a function urea concentration.

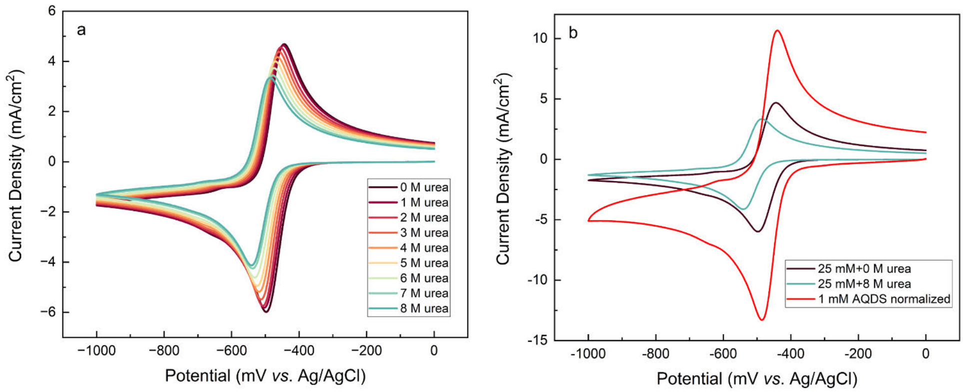

Figure 28. a) Viscosity corrected CV of 25 mM AQDS in 1 M sodium carbonate buffer pH 9.5 at the scan rate of 100 mV/s, b) comparison of CVs for 25 mM AQDS without and with 8 M urea (viscosiy corrected) with normalized CV of 1 mM AQDS (multiplied by 25).

RDE results in Figure 29 also showed that concentrated AQDS solutions exhibited lower limiting currents compared to dilute solutions. Addition of 2 M urea partially restored the limiting current that is an indication of aggregation suppression and an increase in the electrochemically accessible fraction of AQDS from ~76% to ~86% could be measured.

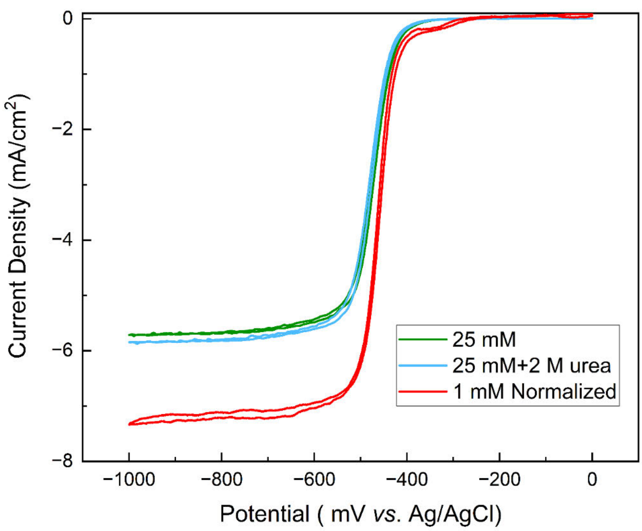

Figure 29. RDE of 25 mM and 1 mM AQDS without and with urea (viscosity corrected) in 1 M sodium carbonate buffer pH 9.5 at the scan rate of 1 mV/s.

Finally, at the battery level, flow battery measurements in Figure 30 confirmed that urea had little influence on the electrochemical performance of AQDS. In the absence of urea, capacity utilization was 58% at 60 mA cm^{-2}. The addition of urea resulted in a nearly identical capacity utilization of 59% at 60 mA cm^{-2} despite RDE results indicating that a higher accessible capacity should be achieved. While coulombic efficiency remained unaffected upon adding urea, EE decreased to 58% from 70% likely due to slower kinetics of the ferro/ferricyanide couple or hindered mass transport in the more viscous electrolytes with urea. These findings demonstrate that although urea can disrupt aggregation at the molecular scale, its advantages do not translate into meaningful improvements in flow batteries.

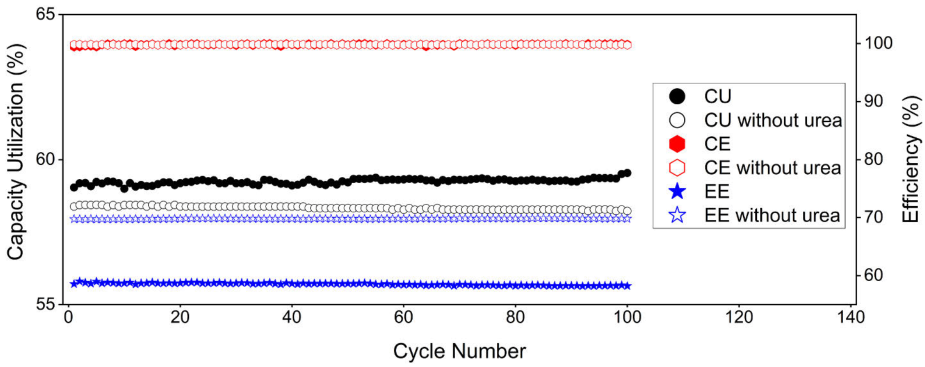

Figure 30. Flow battery performance of 20 mL of 25 mM AQDS/50 mL of 25 mM $Na_4[Fe(CN)_6]$)in 1 M sodium carbonate buffer pH 9.5 with and without urea.

5 Conclusions and Outlook

This thesis focused on the development and electrochemical characterization of RAOMs for AOFBs with particular emphasis on NDI derivatives. Two new water-soluble NDIs namely GABA-NDI and ASP-NDI were synthesized in a single-step reaction and structural characterization by NMR confirmed their successful synthesis. Solubility studies showed that ASP-NDI is nearly twice as soluble as GABA-NDI due to the additional carboxyl group in its structure with solubility of 1.07 M and 0.58 M in water, respectively. This highlights the effect of the functionalization on improving the solubility. Electrochemical measurements revealed that both NDIs undergo two reversible one-electron redox processes with diffusion coefficients on the order of 10^{-6} cm^2/s that makes them suitable for flow batteries. Flow battery tests on GABA-NDI showed that this molecule can achieve high capacity utilization in inert and buffered conditions but suffered from stability issues in unbuffered or oxygen-exposed environments due to the pH change and air sensitivity. Flow battery tests on ASP-NDI demonstrated excellent cycling stability particularly when paired with Fumasep E-630(K) membrane that effectively suppressed ferrocyanide crossover. At the concentration of 500 mM, ASP-NDI flow battery showed a capacity fade of only 0.0275% per day that is the lowest fade rate reported to date for NDI-based flow batteries. After Long-term flow battery tests, both of the studied NDIs did not undergo detectable chemical degradation and their self-association was found to not affect the full utilization of the two-electron process. Overall, these studies established the ASP-NDI as a promising candidate for the near neutral AOFBs.

In addition, this thesis investigated the self-association behaviour of AQDS and NDIs and the potential of urea as a chaotropic agent to mitigate this behaviour. NMR studies confirmed that both AQDS and NDIs undergo π-π stacking at higher concentrations that leads to characteristic upfield chemical shifts and peak broadening. The addition of urea in the molecular level as proved by NMR, disrupted the self-association with the peaks shifting closer to those of dilute solutions and signals sharpening. For AQDS, RDE measurements quantified an increase in the electrochemically accessible fraction from ~76% to ~86% in the presence of urea.

However, flow battery experiments demonstrated that these molecular-level improvements did not translate into meaningful performance gains.

In conclusion, this thesis shows how molecular design and electrolyte composition can influence the performance of AOFBs. It demonstrates that functional group engineering is a powerful tool to enhance solubility and stability of RAOMs. It also reveals that aggregation remains a significant barrier for AQDS-based systems. Although, additives such as urea can provide some levels of disruption at molecular-level, they can compromise flow battery performance or have very little benefits on the performance.

Future work building on this thesis could focus on designing NDI molecules with even higher solubilities than the ASP-NDI and also developing membranes with enhanced selectivity and stability to better mitigate crossover. Osmotic effects should also be monitored during cycling and addressed through suitable electrolyte rebalancing strategies. In addition, operando spectroscopic techniques could provide valuable insights into aggregation dynamics under realistic operating conditions helping to bridge the gap between molecular-scale phenomena and battery-level performance. Finally, the aggregation behaviour of molecules in their reduced states should be studied as this may influence the electrochemical accessibility and long-term stability of the molecules in flow batteries.

Acknowledgements

The research presented in this thesis was done between 2020 and 2024 at the Materials Engineering unit of the University of Turku. The work corresponding to **Publication II** was carried out entirely at DTU Energy in 2023. I acknowledge the financial support provided by the Research Council of Finland through the BioFlow project (Grant agreement No. 343493), the Nordic Flow Battery Network (project-100815), the Turku University Foundation, and the University of Turku Graduate School.

First and foremost, I would like to express my gratitude to my supervisor, Professor Pekka Peljo, for not only accepting me as a doctoral student but also for his invaluable guidance and financial support throughout my doctoral journey.

I am also sincerely thankful to Professor Johan Hjelm for his support and supervision during my research visit at DTU Energy.

A special acknowledgment goes to my mentor, Dr. Cedrik Wiberg, who has consistently guided and supported me since he joined the group in February 2021. His mentorship has played a crucial role in all of the publications and without his support this journey would have been more difficult.

I am deeply grateful to my current supervisor, Professor Jovana Milić, for her belief in my potential. I am also thankful for her guidance and encouragement during the writing and finalization phases of this thesis.

Additionally, I am thankful to Professor Michael Aziz for the discussions during my time in Denmark which were both inspiring and motivating.

I would also like to extend my thanks to the colleagues who made this journey memorable for me (Sachin, Kuldeep, Yusuke, Baichen, Silver, Ulriika, Irene). Last but not the least, special thanks go to Aapo for being my best friend in Finland; thank you for all of the shared moments and support.

Finally, my heartfelt thanks go to my family; Maman, Baba, Sadra, Madarjon, Zahra; for their constant love, encouragement and support from Iran. I am profoundly thankful for their faith in me throughout this journey.

Turku, November 2025
Mahsa Shahsavan

List of References

1. Luo, X., Wang, J., Dooner, M. & Clarke, J. Overview of current development in electrical energy storage technologies and the application potential in power system operation. *Appl. Energy* 137, 511–536 (2015).
2. Weber, A. Z. *et al.* Redox flow batteries: a review. *J. Appl. Electrochem.* 41, 1137–1164 (2011).
3. Soloveichik, G. L. Flow Batteries: Current Status and Trends. *Chem. Rev.* 115, 11533–11558 (2015).
4. Zhu, F., Chen, Q. & Fu, Y. Perspectives on aqueous organic redox flow batteries. *Green Energy Environ.* 9, 1641–1649 (2024).
5. Pan, F. & Wang, Q. Redox Species of Redox Flow Batteries: A Review. *Molecules* 20, 20499–20517 (2015).
6. Shoaib, M. *et al.* Advances in Redox Flow Batteries – A Comprehensive Review on Inorganic and Organic Electrolytes and Engineering Perspectives. *Adv. Energy Mater.* 14, 2400721 (2024).
7. Olabi, A. G. *et al.* Redox Flow Batteries: Recent Development in Main Components, Emerging Technologies, Diagnostic Techniques, Large-Scale Applications, and Challenges and Barriers. *Batteries* 9, 409 (2023).
8. Winsberg, J., Hagemann, T., Janoschka, T., Hager, M. D. & Schubert, U. S. Redox-Flow Batteries: From Metals to Organic Redox-Active Materials. *Angew. Chem. Int. Ed.* 56, 686–711 (2017).
9. Darling, R. M., Gallagher, K. G., Kowalski, J. A., Ha, S. & Brushett, F. R. Pathways to low-cost electrochemical energy storage: a comparison of aqueous and nonaqueous flow batteries. *Energy Environ. Sci.* 7, 3459–3477 (2014).
10. Kwabi, D. G. *et al.* Alkaline Quinone Flow Battery with Long Lifetime at pH 12. *Joule* 2, 1894–1906 (2018).
11. Goulet, M.-A. & Aziz, M. J. Flow Battery Molecular Reactant Stability Determined by Symmetric Cell Cycling Methods. *J. Electrochem. Soc.* 165, A1466 (2018).
12. DeBruler, C., Hu, B., Moss, J., Luo, J. & Liu, T. L. A Sulfonate-Functionalized Viologen Enabling Neutral Cation Exchange, Aqueous Organic Redox Flow Batteries toward Renewable Energy Storage. *ACS Energy Lett.* 3, 663–668 (2018).
13. Luo, J., Hu, B., Hu, M., Zhao, Y. & Liu, T. L. Status and Prospects of Organic Redox Flow Batteries toward Sustainable Energy Storage. *ACS Energy Lett.* 4, 2220–2240 (2019).
14. Wiberg, C., Carney, T. J., Brushett, F., Ahlberg, E. & Wang, E. Dimerization of 9,10-anthraquinone-2,7-Disulfonic acid (AQDS). *Electrochimica Acta* 317, 478–485 (2019).
15. Wiberg, C., Owusu, F., Wang, E. & Ahlberg, E. Electrochemical Evaluation of a Napthalene Diimide Derivative for Potential Application in Aqueous Organic Redox Flow Batteries. *Energy Technol.* 7, 1900843 (2019).
16. Sánchez-Díez, E. *et al.* Redox flow batteries: Status and perspective towards sustainable stationary energy storage. *J. Power Sources* 481, 228804 (2021).
17. Pileri, F., Da Silva Freitas, W., D'Epifanio, A. & Mecheri, B. Advances in organic electroactive species for enhancing the performance of all-aqueous redox flow batteries in electrochemical energy storage. *J. Energy Storage* 113, 115677 (2025).
18. Brushett, F. R., Vaughey, J. T. & Jansen, A. N. An All-Organic Non-aqueous Lithium-Ion Redox Flow Battery. *Adv. Energy Mater.* 2, 1390–1396 (2012).
19. Shahsavan, M., Wiberg, C. & Peljo, P. Gamma-aminobutyric acid-functionalized naphthalene diimide for aqueous organic flow batteries. *Chem. Commun.* 58, 12692–12695 (2022).

20. Huo, Y., Xing, X., Zhang, C., Wang, X. & Li, Y. An all organic redox flow battery with high cell voltage. *RSC Adv.* 9, 13128–13132 (2019).
21. Gerhardt, M. R. *et al.* Anthraquinone Derivatives in Aqueous Flow Batteries. *Adv. Energy Mater.* 7, 1601488 (2017).
22. Jin, S. *et al.* Near Neutral pH Redox Flow Battery with Low Permeability and Long-Lifetime Phosphonated Viologen Active Species. *Adv. Energy Mater.* 10, 2000100 (2020).
23. Kerr, E. F. *et al.* High Energy Density Aqueous Flow Battery Utilizing Extremely Stable, Branching-Induced High-Solubility Anthraquinone near Neutral pH. *ACS Energy Lett.* 8, 600–607 (2023).
24. Amini, K. *et al.* An Extremely Stable, Highly Soluble Monosubstituted Anthraquinone for Aqueous Redox Flow Batteries. *Adv. Funct. Mater.* 33, 2211338 (2023).
25. Wiberg, C., Evenäs, L., Busch, M. & Ahlberg, E. Naphthalene diimides (NDI) in highly stable pH-neutral aqueous organic redox flow batteries. *J. Electroanal. Chem.* 896, 115224 (2021).
26. Huskinson, B. *et al.* A metal-free organic–inorganic aqueous flow battery. *Nature* 505, 195–198 (2014).
27. Yang, Z. *et al.* Alkaline Benzoquinone Aqueous Flow Battery for Large-Scale Storage of Electrical Energy. *Adv. Energy Mater.* 8, 1702056 (2018).
28. Ji, Y. *et al.* A Phosphonate-Functionalized Quinone Redox Flow Battery at Near-Neutral pH with Record Capacity Retention Rate. *Adv. Energy Mater.* 9, 1900039 (2019).
29. Tong, L. *et al.* Molecular Engineering of an Alkaline Naphthoquinone Flow Battery. *ACS Energy Lett.* 4, 1880–1887 (2019).
30. Wu, M. *et al.* Extremely Stable Anthraquinone Negolytes Synthesized from Common Precursors. *Chem* 6, 1432–1442 (2020).
31. Wu, M. *et al.* Highly Stable, Low Redox Potential Quinone for Aqueous Flow Batteries. *Batter. Supercaps* 5, e202200009 (2022).
32. Alfaraidi, A. M. *et al.* An Extremely Stable and Soluble NH_2-Substituted Anthraquinone Electrolyte for Aqueous Redox Flow Batteries. *ACS Appl. Energy Mater.* 6, 12259–12266 (2023).
33. Liu, T., Wei, X., Nie, Z., Sprenkle, V. & Wang, W. A Total Organic Aqueous Redox Flow Battery Employing a Low Cost and Sustainable Methyl Viologen Anolyte and 4-HO-TEMPO Catholyte. *Adv. Energy Mater.* 6, 1501449 (2016).
34. Gentil, S., Reynard, D. & Girault, H. H. Aqueous organic and redox-mediated redox flow batteries: a review. *Curr. Opin. Electrochem.* 21, 7–13 (2020).
35. Singh, V., Kim, S., Kang, J. & Byon, H. R. Aqueous organic redox flow batteries. *Nano Res.* 12, 1988–2001 (2019).
36. DeBruler, C. *et al.* Designer Two-Electron Storage Viologen Anolyte Materials for Neutral Aqueous Organic Redox Flow Batteries. *Chem* 3, 961–978 (2017).
37. Beh, E. S. *et al.* A Neutral pH Aqueous Organic–Organometallic Redox Flow Battery with Extremely High Capacity Retention. *ACS Energy Lett.* 2, 639–644 (2017).
38. Li, H. *et al.* Spatial Structure Regulation: A Rod-Shaped Viologen Enables Long Lifetime in Aqueous Redox Flow Batteries. *Angew. Chem.* 133, 27177–27183 (2021).
39. Tang, G. *et al.* Designing Robust Two-Electron Storage Extended Bipyridinium Anolytes for pH-Neutral Aqueous Organic Redox Flow Batteries. *JACS Au* 2, 1214–1222 (2022).
40. Peng, K., Sun, P., Yang, Z. & Xu, T. A PEGylated Viologen for Crossover-Free and High-Capacity pH-Neutral Aqueous Organic Redox Flow Batteries. *Batter. Supercaps* 6, e202200426 (2023).
41. Mohapatra, S. K., Ramanujam, K. & Sethuraman, S. Tracking and Tackling the Capacity Fading in Viologen based Aqueous Organic Redox Flow Batteries. *J. Electrochem. Soc.* 172, 010523 (2025).
42. Wiberg, C., Busch, M., Evenäs, L. & Ahlberg, E. The electrochemical response of core-functionalized naphthalene Diimides (NDI) – a combined computational and experimental investigation. *Electrochimica Acta* 367, 137480 (2021).
43. Wang, Z. *et al.* Realizing one-step two-electron transfer of naphthalene diimides *via* a regional charge buffering strategy for aqueous organic redox flow batteries. *Mater. Horiz.* 11, 1283–1293 (2024).

44. Medabalmi, V., Sundararajan, M., Singh, V., Baik, M.-H. & Ryung Byon, H. Naphthalene diimide as a two-electron anolyte for aqueous and neutral pH redox flow batteries. *J. Mater. Chem. A* 8, 11218–11223 (2020).
45. Singh, V., Ahn, S. & Byon, H. R. Ammonium-Functionalized Naphthalene Diimides as Two-Electron-Transfer Negolyte for Aqueous Redox Flow Batteries. *Batter. Supercaps* 5, e202200281 (2022).
46. Pan, M. *et al.* High-voltage and durable pH-neutral aqueous redox flow batteries based on quaternary ammonium cations functionalized naphthalene diimide and nitroxyl radical systems. *J. Power Sources* 580, 233269 (2023).
47. Singh, V. *et al.* Controlling π–π Interactions of Highly Soluble Naphthalene Diimide Derivatives for Neutral pH Aqueous Redox Flow Batteries. *Adv. Mater.* 35, 2210859 (2023).
48. Liu, X. *et al.* Commercializable Naphthalene Diimide Anolytes for Neutral Aqueous Organic Redox Flow Batteries. *Angew. Chem. Int. Ed.* 63, e202405427 (2024).
49. Zhang, H. *et al.* Synergistic ionic modification strategy enhances the stability of naphthalene diimide zwitterions for cost-effective aqueous organic redox flow batteries. *Natl. Sci. Rev.* 12, nwaf123 (2025).
50. Zhang, X. *et al.* Multi-hydrogen bond engineered imidazolium-functionalized naphthalene diimides for stable two-electron storage in aqueous organic flow batteries. *Energy Storage Mater.* 81, 104527 (2025).
51. Carney, T. J., Collins, S. J., Moore, J. S. & Brushett, F. R. Concentration-Dependent Dimerization of Anthraquinone Disulfonic Acid and Its Impact on Charge Storage. *Chem. Mater.* 29, 4801–4810 (2017).
52. Pasadakis-Kavounis, A., Baj, V. & Hjelm, J. Aggregation and Capacity Limiting Effects in Anthraquinone-Based Flow Battery Negolytes. *J. Electrochem. Soc.* 171, 020501 (2024).
53. Geraskina, M. R., Dutton, A. S., Juetten, M. J., Wood, S. A. & Winter, A. H. The Viologen Cation Radical Pimer: A Case of Dispersion-Driven Bonding. *Angew. Chem. Int. Ed.* 56, 9435–9439 (2017).
54. Dalvand, P. *et al.* Viologen–cucurbituril host/guest chemistry – redox control of dimerization versus inclusion. *RSC Adv.* 11, 29543–29554 (2021).
55. Kim, M., Kim, Y. M. & Moon, H. C. Asymmetric molecular modification of viologens for highly stable electrochromic devices. *RSC Adv.* 10, 394–401 (2019).
56. Ashok, A. & Kumar, A. A comprehensive review of metal-based redox flow batteries: progress and perspectives. *Green Chem. Lett. Rev.* 17, 2302834 (2024).
57. Arévalo-Cid, P., Dias, P., Mendes, A. & Azevedo, J. Redox flow batteries: a new frontier on energy storage. *Sustain. Energy Fuels* 5, 5366–5419 (2021).
58. Asenjo-Pascual, J. *et al.* Understanding Aqueous Organic Redox Flow Batteries: A Guided Experimental Tour from Components Characterization to Final Assembly. *Batteries* 8, 193 (2022).
59. Sun, J., Shi, D., Zhong, H., Li, X. & Zhang, H. Investigations on the self-discharge process in vanadium flow battery. *J. Power Sources* 294, 562–568 (2015).
60. Al-Sakaji, B. A. K., Husseini, G. A. & Darwish, N. A. Impact of Ionic Strength and Charge Density on Donnan Potential in the NaCl-Cation Exchange Membrane System. *Water* 15, 3830 (2023).
61. Wu, W., Wang, A. P., Luo, J. & Liu, T. L. A Highly Stable, Capacity Dense Carboxylate Viologen Anolyte towards Long-Duration Energy Storage. *Angew. Chem. Int. Ed.* 62, e202216662 (2023).
62. Kim, M. B. & Dixon, D. W. Hydrolysis of aliphatic naphthalene diimides: effect of charge placement in the side chains. *J. Phys. Org. Chem.* 21, 731–737 (2008).
63. Tang, G., Yang, Z. & Xu, T. Two-electron storage electrolytes for aqueous organic redox flow batteries. *Cell Rep. Phys. Sci.* 3, 101195 (2022).
64. Salmeron-Sanchez, I. *et al.* Chemical physics insight of PPy-based modified ion exchange membranes: A fundamental approach. *J. Membr. Sci.* 643, 120020 (2022).
65. Van Cauter, C. J., Li, Y., Van Herck, S. & Vankelecom, I. F. J. Stability and Performance of Commercial Membranes in High-Temperature Organic Flow Batteries. *Membranes* 14, 177 (2024).

66. Small, L. J., Pratt, H. D. & Anderson, T. M. Crossover in Membranes for Aqueous Soluble Organic Redox Flow Batteries. *J. Electrochem. Soc.* 166, A2536–A2542 (2019).
67. Oh, K., Moazzam, M., Gwak, G. & Ju, H. Water crossover phenomena in all-vanadium redox flow batteries. *Electrochimica Acta* 297, 101–111 (2019).
68. Moelbert, S., Normand, B. & De Los Rios, P. Kosmotropes and chaotropes: modelling preferential exclusion, binding and aggregate stability. *Biophys. Chem.* 112, 45–57 (2004).
69. Peljo, P. *et al.* Effect of Chaotropes on the Transfer of Ions and Dyes across the Liquid–Liquid Interface. *J. Phys. Chem. C* 122, 18510–18519 (2018).
70. Bourdon, R. *et al.* Chaotropic agents boosting the performance of photoionic cells. *J. Phys. Chem. C* 119, 4728–4735 (2015).

TURUN
YLIOPISTO
UNIVERSITY
OF TURKU

Painosalama, Turku, Finland 2025

ISBN 978-952-02-0475-4 (PDF)
ISSN 2736-9390 (Painettu/Print)
ISSN 2736-9684 (Sähköinen/Online)